(2)

AD ____

CONTRACT NO: DAMD17-89-C-9063

Original contains color plates: All DTIC reproductions will be in black and white

TITLE: DETERMINATION BY X-RAY CRYSTALLOGRAPHY OF THE THREE-DIMENSIONAL STRUCTURE OF ACETYLCHOLINESTERASE FROM TORPEDO ELECTRIC ORGAN

PRINCIPAL INVESTIGATORS: J.L. SUSSMAN, Ph.D.
I. SILMAN, Ph.D.

CONTRACTING ORGANIZATION: Weizmann Institute of Science
Departments of Structural Biology & Neurobiology
Rehovot 76100, Israel

REPORT DATE: April 17, 1993

TYPE OF REPORT: Final Report

PREPARED FOR: U.S. Army Medical Research and Development Command
Fort Detrick, Frederick, MD 21702-5012

DISTRIBUTION STATEMENT: Approved for public release;
distribution unlimited.

The findings in this report are not to be construed as an official Department of the Army position unless so designated by other authorized documents.

AD _____

CONTRACT NO: DAMD17-89-C-9063

TITLE: DETERMINATION BY X-RAY CRYSTALLOGRAPHY OF THE THREE-DIMENSIONAL STRUCTURE OF ACETYLCHOLINESTERASE FROM TORPEDO ELECTRIC ORGAN

PRINCIPAL INVESTIGATORS: J.L. SUSSMAN, Ph.D.
I. SILMAN, Ph.D.

CONTRACTING ORGANIZATION: Weizmann Institute of Science
Departments of Structural Biology & Neurobiology
Rehovot 76100, Israel

REPORT DATE: April 17, 1993

TYPE OF REPORT: Final Report

PREPARED FOR: U.S. Army Medical Research and Development Command
Fort Detrick, Frederick, MD 21702-5012

SECURITY CLASSIFICATION OF THIS PAGE

REPORT DOCUMENTATION PAGE

Form Approved
OMB No. 0704-0188

1a. REPORT SECURITY CLASSIFICATION Unclassified	1b. RESTRICTIVE MARKINGS
2a. SECURITY CLASSIFICATION AUTHORITY	3. DISTRIBUTION/AVAILABILITY OF REPORT Approved for public release; distribution unlimited
2b. DECLASSIFICATION/DOWNGRADING SCHEDULE	
4. PERFORMING ORGANIZATION REPORT NUMBER(S)	5. MONITORING ORGANIZATION REPORT NUMBER(S)
6a. NAME OF PERFORMING ORGANIZATION Weizmann Institute of Science 6b. OFFICE SYMBOL (If applicable)	7a. NAME OF MONITORING ORGANIZATION
6c. ADDRESS (City, State, and ZIP Code) Departments of Structural Biology and Neurobiology Rehovot 76100 Israel	7b. ADDRESS (City, State, and ZIP Code)
8a. NAME OF FUNDING/SPONSORING ORGANIZATION Medical Research & Develop. Com 8b. OFFICE SYMBOL (If applicable)	9. PROCUREMENT INSTRUMENT IDENTIFICATION NUMBER Contract No. DAMD17-89-9063
8c. ADDRESS (City, State, and ZIP Code) Fort Detrick Frederick, MD 21702-5012	10. SOURCE OF FUNDING NUMBERS PROGRAM ELEMENT NO. 61102A; PROJECT NO. 30161102BS11; TASK NO. AA; WORK UNIT ACCESSION NO. 019

11. TITLE (Include Security Classification)
Determination by X-ray Crystallography of the Three-dimensional Structure of Acetylcholinesterase from Torpedo Electric Organ

12. PERSONAL AUTHOR(S)
Profs. J.L. Sussman and I. Silman

13a. TYPE OF REPORT	13b. TIME COVERED	14. DATE OF REPORT (Year, Month, Day)	15. PAGE COUNT
Final	FROM 3/27/89 TO 12/31/92	1993 April 17	63

16. SUPPLEMENTARY NOTATION

17. COSATI CODES			18. SUBJECT TERMS (Continue on reverse if necessary and identify by block number)
FIELD	GROUP	SUB-GROUP	Acetylcholinesterase; X-ray Crystallography; Electric Ray;

19. ABSTRACT (Continue on reverse if necessary and identify by block number)

The X-ray structure of *Torpedo californica* acetylcholinesterase (AChE) was determined. The active site lies near the bottom of a deep cavity: the *aromatic gorge*. The choline-binding subsite contains one negative charge, and modelling reveals that the quaternary group of acetylcholine interacts principally with the indole of W84. X-ray structures of complexes of AChE with edrophonium and tacrine show that both interact with W84. The structure of a complex with the *bis*quaternary inhibitor, 1,5-*bis*(4-allyldimethylammoniumphenyl)pentane-3-one, shows that one quaternary nitrogen interacts with W84, while the distal quaternary nitrogen interacts with W279, thus establishing the location of the 'peripheral' binding site.

Human butyrylcholinesterase (BChE) was modelled on the basis of AChE. It closely resembles AChE; two aromatics, F288 and F290, replaced by Leu and Val, respectively, in BChE, may prevent entrance of butyrylcholine into the acyl-binding pocket. Site-directed mutagenesis produced a double mutant, F288L/F290V, which hydrolyzes both butyrylthiocholine and acetylthiocholine, and is inhibited by the BChE-specific organophosphate, isoOMPA. Another mutant, W279A, displays reduced inhibition, relative to the wild type, by the peripheral-site ligand, propidium, whereas inhibition by edrophonium is unaffected, corroborating the assignment of the peripheral anionic site.

20. DISTRIBUTION/AVAILABILITY OF ABSTRACT	21. ABSTRACT SECURITY CLASSIFICATION
☐ UNCLASSIFIED/UNLIMITED ☒ SAME AS RPT. ☐ DTIC USERS	Unclassified

22a. NAME OF RESPONSIBLE INDIVIDUAL	22b. TELEPHONE (Include Area Code)	22c. OFFICE SYMBOL
Virginia Miller	301-619-7328	SGRD-RMI-S

FOREWORD

Options, interpretations, conclusions and recommendations are those of the author and are not necessarily endorsed by the U.S. Army.

_____ Where copyrighted material is quoted, permission has been obtained to use such material.

_____ Where material from documents designed for limited distribution is quoted, permission has been obtained to use the material.

_____ Citations of commercial organizations and trade names in this report do not constitute an official Department of the Army endorsement or approval of the products or services of these organizations.

_____ In conducting research using animals, the investigator(s) adhered to the "Guide for the Care and Use of Laboratory Animals," prepared by the Committee on Care and Use of Laboratory Animals of the Institute of Laboratory Resources, National Research Council (NIH Publication No. 86-23, Revised 1985).

_____ For the protection of human subjects, the investigator(s) adhered to policies of applicable Federal Law 45 CFR 46.

_____ In conducting research utilizing recombinant DNA technology, the investigator(s) adhered to current guidelines promulgated by the National Institutes of Health.

Frank Selman 12/21/93

PI - Signature DATE

SUMMARY

The objective of this project was to solve, for the first time, by X-ray crystallography, the three-dimensional structure of acetylcholinesterase and to learn from this structure the reaction mechanism, inhibition modes, and other structural and functional properties of the enzyme.

The three-dimensional structure of acetylcholinesterase (AChE) from *Torpedo californica* electric organ was determined by X-ray analysis to 2.8 Å resolution (Sussman *et al.* (1991) *Science*, **253**, 872-879). The form crystallized is the glycolipid-anchored homodimer purified subsequent to solubilization with a bacterial phosphatidylinositol-specific lipase C (Sussman *et al.* (1988) *J. Mol. Biol.*, **203**, 821-823). The enzyme monomer is an α/β protein, containing 537 amino acids. It consists of an 12-stranded mixed β-sheet, surrounded by 14 α-helices and bears a striking resemblance to several hydrolase structures including dienelactone hydrolase, serine carboxypeptidase-II, three neutral lipases and haloalkane dehalogenase. The active site is unusual because it contains Glu, not Asp, in the Ser-His-Acid catalytic triad, and because the relationship of the triad to the rest of the protein approximates a mirror image of that seen in the serine proteases. Furthermore, the active site lies near the bottom of a deep and narrow cavity, which we have named the aromatic gorge, since it is lined by rings of 14 conserved aromatic amino acids. The choline binding 'anionic' subsite itself is misnamed, as it contains at most one formal negative charge. Instead the quaternary moiety of choline appears to bind chiefly through interactions with the π electrons in the aromatic residues on AChE. The gorge is so deep, and its aromatic surface so extensive, that there must be many different ways and places for substrate, agonists, and inhibitors to bind to AChE. However, modeling of ACh binding to the enzyme suggests that the principal interaction of the quaternary group is with the indole ring of Trp84.

X-ray refined structures of complexes of *Torpedo californica* AChE with edrophonium and tacrine (Sussman, Harel & Silman (1992), in *Multidisciplinary Approaches to Cholinesterase Functions* , Shafferman & Velan, Eds., pp. 95-107) have shown both ligands to be opposed to Trp84. A second conserved aromatic ring, that of Phe330, undergoes a conformational change so as to make an aromatic-aromatic or aromatic-quaternary interaction with the bound ligand. A similar conformation change in the indole ring of Trp279, at the opening of the gorge, ~18 Å away from the 'anionic' binding site, indicates a possible location for the 'peripheral' anionic site.

X-ray structure refinement, at 2.9 Å resolution, of the complex of AChE with the *bis*quaternary inhibitor 1,5-*bis*(4-allydimethylammoniumphenyl)pentane-3-one dibromide

(BW284c51), which spans the aromatic gorge, shows the interaction of one *bis*quaternary nitrogen with the inner Trp84, in a fashion similar to the two *mono*quaternary ligands, while the second quaternary nitrogen interacts with Trp279, thus confirming the location of the 'peripheral' binding site of AChE.

Torpedo AChE and human butyrylcholinesterase (BChE), while clearly differing in substrate specificity and sensitivity to various inhibitors, possess 53% sequence homology. This permitted modeling of human BChE on the basis of the three-dimensional structure of *Torpedo* AChE (Harel *et al.* (1992) *Proc. Natl. Acad. Sci. USA*, **89**, 10827-10831). The modeled BChE structure closely resembled that of AChE in overall features. However, six of the aromatic residues which are conserved in the active site gorge of AChE are absent in BChE. Modeling showed that two such residues, Phe288 and Phe290, which are replaced by Leu and Val, respectively, in BChE, may prevent entrance of butyrylcholine (BCh) into the acyl-binding pocket. We generated, by site-directed mutagenesis, a double mutant, Phe288Leu/Phe290Val, in which the aromatic residues of *Torpedo* AChE are replaced by the aliphatic residues present in human BChE. This mutant hydrolyzes butyrylthiocholine as well as acetylthiocholine, and is inhibited very efficiently by the BChE-specific organophosphate isoOMPA. The enhanced potency of *bis*quaternary compounds relative to the corresponding *mono*quaternary ligands does not hold for BChE. The replacement of Trp279 by Ala in BChE might explain its lack of a 'peripheral' site, and thus its failure to display enhanced sensitivity to *bis*quaternary inhibitors. The mutant, Trp279Ala, displayed strongly reduced inhibition, relative to the wild type, by the peripheral-site-specific ligand, propidium, whereas inhibition by the catalytic site inhibitor was unaffected. This adds additional support to the assignment of Trp279 to the peripheral anionic site in *Torpedo* AChE.

TABLE OF CONTENTS

I) OBJECTIVES

The objective of this proposal was to determine the three-dimensional structure of acetylcholinesterase (AChE) from *Torpedo californica* at atomic resolution. This was approached by the method of single-crystal X-ray diffraction. The project entailed the following steps:

a) Development of a routine procedure for obtaining large quantities of highly purified AChE by affinity chromatography followed by HPLC.
b) Development of reproducible procedures for growing large and highly ordered single crystals of AChE suitable for high-resolution X-ray diffraction.
c) Utilization of cryogenic data collection on an area detector for accurate and rapid collection of X-ray intensities.
d) Preparation of isomorphous heavy atom derivatives of the AChE crystals, so as to permit solution of the phase problem.
e) Employment of real-time computer graphics to trace the backbone fold of AChE in the electron density map, based on the method of multiple isomorphous replacements (MIR) phases.
f) Least-squares refinement of the entire structure to fit the observed X-ray data.

II) BACKGROUND

The principal biological role of AChE is termination of impulse transmission at cholinergic synapses by rapid hydrolysis of the neurotransmitter acetylcholine (ACh) (1).

$$CH_3COOCH_2CH_2N^+(CH_3)_3 + AChE$$
$$\downarrow$$
$$CH_3CO\text{-}AChE + HOCH_2CH_2N^+(CH_3)_3$$
$$\downarrow$$
$$CH_3COO^- + H^+ + AChE$$

In keeping with this requirement, AChE possesses a remarkably high specific activity, especially for a serine hydrolase (for a review, see (2)), functioning at a rate approaching that of a diffusion-controlled reaction (3). The powerful acute toxicity of organophosphorus poisons (as well as of carbamates and sulfonyl halides which function analogously) is primarily due to the fact that they serve as potent inhibitors of AChE (4). Inhibition results from the formation of a covalent bond with a serine residue in the active site (2). AChE inhibitors are used in treatment of various disorders such as myasthenia gravis and glaucoma (5), and their use has been proposed as a possible therapeutic approach to the management of Alzheimer's disease (6). Knowledge of the three-dimensional structure of AChE is, therefore, essential for understanding its remarkable catalytic efficacy, for rational drug design, and for developing therapeutic approaches to organophosphate poisoning. Furthermore, information about the ACh-binding site of AChE will help us understand the molecular basis for the recognition of ACh by other ACh-binding proteins such as the various ACh receptors (7).

The different oligomeric forms of AChE in the electric organ of the electric fish, *Electrophorus* and *Torpedo*, are structurally homologous to those in vertebrate nerve and muscle (8). Highly purified preparations from these abundant sources of AChE (9) have taught us much about the number and arrangement of subunits and modes of anchoring to the surface membrane of these molecular forms (10). They have also yielded considerable information concerning the surface topography of AChE (11) and about its mechanism of action (2).

Early kinetic studies indicated that the active site of AChE contains two subsites, the 'esteratic' and 'anionic' subsites (12), corresponding, respectively, to the catalytic machinery and the choline-binding pocket. The 'esteratic' subsite is believed to resemble the catalytic subsites of other serine hydrolases (13, 14). The active-site serine, with which organophosphates react, has

been unequivocally established to be Ser200 in *T. californica* AChE (15). Both kinetic and chemical studies (16) implicate a histidine residue in the active site. The 'anionic' subsite binds the charged quaternary group of the choline moiety of ACh, and is believed to bind both quaternary ligands, such as edrophonium (17) and *N*-methylacridinium (18), which act as competitive inhibitors, and quaternary oximes, which often serve as effective reactivators of organophosphate-inhibited AChE (13). Cohen and coworkers (19) have suggested, on the basis of studies employing cationic and uncharged homologs of ACh, that the 'anionic' subsite is, in fact, uncharged and lipophilic. Furthermore, chemical modification and spectroscopic studies support the presence of aromatic residues in the active site of AChE (20-22).

In addition to the two subsites of the catalytic center, AChE possesses one or more binding sites for ACh and other quaternary ligands (Figure 3). Such 'peripheral' anionic site(s), clearly distinct from the choline-binding pocket of the active site, have been proposed (18, 23, 24) and were firmly established by Taylor & Lappi (25) by use of the fluorescent probe, propidium. It acts as an uncompetitive inhibitor and binds at a site clearly distinct from that occupied by the *mono*quaternary competitive inhibitors mentioned above. Radic *et al.* (26) recently provided experimental evidence that this is the site involved in the substrate inhibition characteristic of AChE. For a recent review of this complex literature, see (2).

The first AChE crystals obtained were of a tetrameric form purified from electric organ tissue of *Electrophorus electricus* (27). Although preliminary characterization of these crystals was reported over 25 years ago by Chothia & Leuzinger (28) and, more recently, by Schrag *et al.* (29), no structural data have yet been presented.

In vertebrates, two enzymes efficiently catalyze ACh hydrolysis: AChE and a second enzyme, butyrylcholinesterase (BChE) (30). Although the second enzyme, BChE, is widely distributed, its biological role is unknown (31). BChE is so called since it hydrolyses BCh at rates similar to or faster than ACh, whereas AChE hydrolyses BCh much more slowly than it hydrolyses ACh (31). BChE is also known as serum cholinesterase, due to its high concentration in vertebrate serum (31). The two enzymes are further distinguished by their differential susceptibility to various inhibitors (32). For example, some *bis*quaternary compounds, which are more potent inhibitors of AChE than their *mono*quaternary counterparts, bind poorly to BChE (33). Human BChE (H-BChE) is of interest to anesthesiologists and geneticists, since it is responsible for breakdown of the short-term muscle relaxant, succinylcholine (34), and because numerous genetic variants exist in which the rate of succinylcholine hydrolysis is reduced (31).

III) RESULTS

A) Atomic Structure of Acetylcholinesterase from Torpedo californica

1) Purification, crystallization and structure determination

In *Torpedo*, a major form of AChE is a homodimer bound to the plasma membrane via covalently attached phosphatidylinositol (PI) (10). This dimer has a simpler quaternary structure than *Electrophorus* AChE, and its sequence and the arrangement of its intrachain disulfides have been determined (15, 35, 36). The PI is attached to the COOH-terminus of each monomer through an intervening oligosaccharide, with the diglyceride moiety of the PI serving as the hydrophobic anchor (10). Consequently, the dimer can be selectively solubilized by a bacterial PI-specific phospholipase C (37). This mild procedure also achieves significant purification prior to affinity chromatography. We were thus able to obtain large amounts of pure, un-nicked enzyme for crystallization. We earlier reported preliminary crystallographic characterization of crystals of this form of AChE obtained from polyethyleneglycol (PEG) 200 (38).

Recently we obtained a crystal form more suitable for X-ray analysis. AChE, purified as already described (38), was crystallized at 19°C, using standard vapor diffusion techniques in hanging drops (39) with 61% saturated ammonium sulfate, 360 mM Na, K-phosphate buffer, pH 7.0, as precipitating agent and a protein concentration of ~11 mg/ml (40). Single trigonal crystals grew within a few weeks to dimensions of 0.8 x 0.4 x 0.4 mm (Figure 1). They belong to space group $P3_121$, contain one monomer per asymmetric unit and diffract to 2.6 Å resolution (Figure 2). Compared to the crystal form grown from PEG 200 (38), the trigonal crystals grow more reproducibly, are mechanically more robust and survive longer in the X-ray beam (Table 1).

The structure was solved by the multiple isomorphous replacement (MIR) method (Table 1) followed by three cycles of solvent-flattening (41) and phase combination to improve the map (Figure 4). An initial AChE model comprising 505 out of a total of 537 residues in the polypeptide chain (42) was obtained by applying the fragment retrieval option, DGNL, to fit fragments from the Brookhaven Protein Structure Data Bank (43) to the skeletonised electron density distribution generated by BONES as implemented in the program FRODO (44-46). One of the two mercury sites of the $HgAc_2$ derivative (see Table 1) is buried in the interior of the protein. Biochemical studies had previously shown that several thiol reagents, including the organomercurial, *p*-chloromercurisulfonic acid, inhibit *Torpedo* AChE (47). The sulfhydryl of

Cys231 is the only free thiol in the enzyme (36) and seemed, therefore, a reasonable attachment site for a mercury derivative. Since kinetic constants suggested that the sulfhydryl modified is relatively inaccessible, we searched in the vicinity of the buried mercury atom for densities whose shape corresponded to the sequence Cys231-Pro232-Trp233. When this sequence proved to fit the observed density satisfactorily, we built out from the tripeptide in both directions. The amino acid sequence could be fitted accurately to the electron density at all points, and bifurcations were observed, as might be predicted, at the sites of the three intrachain disulfides (36). The initial R-factor for 15-2.8 Å resolution data, based on these 505 residues, was 43% before any crystallographic refinement.

A preliminary refinement using the simulated annealing program X-PLOR (48), yielded calculated phases that were used to produce a new map which revealed an additional 21 of the missing amino acid residues. Refinement was continued, using X-PLOR in conjunction with PROFFT (49-51), decreasing the R-factor to 18.6% for all data ($F > 0\ \sigma$) from 6.0 to 2.8 Å resolution. The present model, consisting of 526 residues and 71 water molecules, maintains good stereochemistry; it has an r.m.s. deviation in bond lengths of 0.021 Å and in bond angles of 4.0°. 81 atoms, belonging to side-chains of 27 polar surface residues which were not seen in the electron density map even after being omitted, were excluded from the refinement. The coordinates have Accession Number 1ACE in the Brookhaven Protein Data Bank (43).

2) General structure

The molecule has an ellipsoidal shape with dimensions ~45 x 60 x 65 Å. It belongs to the class of α/β proteins (52, 53) and consists of a 12-stranded mixed β-sheet, surrounded by 14 α-helices (Figures 5 & 6). The first and last pairs of strands each form β-hairpin loops which are only loosely hydrogen-bonded to the eight central, superhelically twisted strands (Figure 5B). Viewed along its axis, the central sheet curves ~180Å while viewed perpendicular to its axis, the first and last strands cross each other at ~90Å. Of the 14 helices, two of the longer ones, namely α_F and α_H, are bent close to their interhelix disulfide bridge. The α-helical content of 30% and β-sheet content of 15% observed in the crystal structure are in reasonable agreement with those estimated from CD measurements (54).

The AChE homodimer, whose subunits are related by a crystallographic two-fold axis, appears to be held together by a four-helix bundle composed of helices $\alpha_{F'3}$ and α_H from each subunit (Figure 7). The only interchain disulfide involves the C-terminal Cys537 (36). The three C-terminal residues and the oligoglycan extension of the membrane-anchoring domain (42) are

not visible in the electron density map, most likely because they are disordered. Residues 1-3 and an exposed loop from 485 to 489 are also not seen, presumably for the same reason.

3) Active site

The existence of a catalytic triad in AChE has been the subject of controversy (2). The earlier identification of Ser200 as the active-site serine of *T. californica* AChE (15) has recently been supplemented by the designation of His440 as the catalytic histidine residue on the basis of sequence comparison (55, 56) and site-directed mutagenesis (57). Our chain tracing clearly supports this assignment by placing His440 near Ser200. Glu327 is also near His440. The three residues form a planar array which resembles the catalytic triad of chymotrypsin (Cht) and other serine proteases (58) (Figure 8A). There are, however, two important differences: 1) AChE, together with a neutral lipase from *Geotrichum candidum*, whose three-dimensional structure was also solved only recently (59), are the first published cases of Glu occurring instead of Asp in a catalytic triad. 2) This triad is of opposite 'handedness' to that found in serine proteases. This change in hand is equivalent to keeping the position of the O_γ, the histidine imidazole ring and the acid carboxylate group approximately constant, while rotating the rest of the molecule about the line joining $SerC_\beta$ to $HisC_\gamma$, thus reversing the direction of the polypeptide backbone around the His and Ser residues (Figure 8A). This suggests that the oxyanion hole, which is formed by the amide NH of the active site Ser in the serine proteases (i.e. N-terminal), would be formed by the amide NH of the following residue in AChE, Ala201 (i.e. C-terminal). All three triad residues occur within highly conserved regions of the sequence (Figure 6) and, as is typical of active sites in α/β-proteins (60), are in loops following the C-termini of β-strands.

4) Active site gorge

The most remarkable feature of the *Torpedo* AChE structure is a deep and narrow gorge, about 20 Å long, which penetrates halfway into the enzyme and widens out close to its base (Figure 9A). We have named this cavity the 'active site gorge' because it contains the AChE catalytic triad. O_γ, which can be seen from the surface of the enzyme (Figure 9B), is about 4 Å above the base of the gorge. 14 aromatic residues line a substantial portion of the surface of the gorge (~40%) (Figures 4, 6, 9 & 10). These residues and their flanking sequences, which are highly conserved in AChEs from various species (Figure 6), come primarily from loops between $\beta1$ and $\beta2$, $\beta2$ and $\beta3$, $\beta5$ and $\beta6$, $\beta7$ and $\beta8$, and after $\beta8$ (Figure 5C). Residues as far apart as Asn66 and Ile444 contribute to the lining and base of the gorge, and are all synthesized on the first exon, which codes for residues 1-480 (61). It should be noted that the gorge contains only a

few acidic residues: these include Asp285 and Glu273 at the very top, Asp72, hydrogen-bonded to Tyr334, about half way down, and Glu199, close to the bottom.

The presence of tryptophan in the active site of AChE was predicted by spectroscopic and chemical modification studies (20, 62). The recent affinity labeling study of Weise *et al.* (63) in fact identified Trp84 as part of the putative 'anionic' (choline) binding site. An earlier photoaffinity labeling study implicated a peptide in electric eel AChE, homologous to *Torpedo* Gly328-Ser329-Phe330-Phe331, as part of the binding site (64), and similar data, demonstrating photolabeling of F330 of *T. marmorata* AChE were presented recently (65). The observation of tyrosine residues adjacent to the catalytic site agrees with chemical modification studies (21, 22, 66). The hydroxyl groups of Tyr121 (half-way up) and Tyr130 (at the bottom) point into the gorge.

Despite the structural complexity of the gorge and the flexibility of the natural substrate, ACh (67), a good fit of the extended, all-*trans* conformation of ACh was obtained by manual docking. Specifically, the acyl group was positioned to make a tetrahedral bond with the O_γ of Ser200, while the quaternary group of the choline moiety was placed within van der Waals distance (~3.5 Å) of Trp84 (Figure 8B). This is in striking agreement with the study of Weise *et al.* (63) mentioned above, in which a quaternary affinity label was shown to label Trp84 specifically. Our model suggests that the 'oxyanion hole' (58) would be formed by the main chain nitrogens of Gly118, Gly119 and Ala201 interacting with the carbonyl oxygen, and that the ester oxygen may interact with the imidazole of His440. The fact that the amide nitrogen of Ala201, and not that of Ser200, contributes to the 'oxyanion hole' is consistent with the reversed topology, noted above, of the catalytic triad relative to the serine proteases. Gly118 and Gly119 are part of a 10-residue conserved sequence which contains three glycines in a row; this may make the chain flexible enough to allow amide nitrogens from both Gly118 and Gly119 to be part of the oxyanion hole. Glu199, which might serve as an anionic component of the substrate-binding site, appears, in our model, to make close contacts (~3 Å) both to one of the quaternary methyl groups and to the α-carbon of the choline moiety. We have omitted it from Figure 8B since it has been reported that mutating it to glutamine does not have a dramatic effect on the kinetic parameters (57). Glu199 appears, however, to be hydrogen-bonded, either directly or through a water molecule, to Glu443. Since both carboxylic acid side-chains are in a hydrophobic environment in the interior of AChE, it seems likely that one or both of them may be protonated. This might explain the unexpected result of the mutagenesis experiment.

The high aromatic content of the walls and floor of the active site gorge, together with its dimensions, may help to explain why biochemical studies have revealed a variety of hydrophobic and 'anionic' binding sites distinct from, or overlapping, the active site. For instance, chemical modification by various reagents greatly reduces enzymic activity towards ACh either without affecting, or sometimes actually enhancing, activity towards various neutral esters (66, 68, 69). This supports the existence of hydrophobic areas distinct from the binding site for ACh. Other evidence for hydrophobic sites extending beyond or distinct from the anionic site comes from studies on the affinities and reaction rates of homologous series of organophosphate inhibitors (70), on the affinities of various acridine derivatives (71) and from studies employing resolved enantiomeric methylphosphonothioates (72, 73). The complexity of the array of aromatic residues also provides candidates for a binding site for aromatic cations, the existence of which, closer to the esteratic site than the 'anionic' site, was recently proposed (11). All these results are consistent with the characteristics of the deep gorge extending up from the active site of AChE.

Two reports have used photo labeling (74) and affinity labeling (63) to identify peptide sequences, residues 251-264 and 270-278 respectively, as part of the 'peripheral' binding site(s) for ACh and other quaternary ligands. These two neighboring peptides on the surface of the protein are close to the rim of the gorge. The complex and varied inhibitory effects of different peripheral site ligands (2, 14, 24) may be better understood taking into account the complex geometry of the gorge. Certain ligands may be too bulky to penetrate it, but still might partially block its entrance. The longer *bis*quaternary compounds, which serve as potent inhibitors, might attach at one end to the peripheral site(s) and at the other end to any one of the various aromatic residues lining the walls of the gorge. However, because of its depth, shorter *bis*quaternary inhibitors and oxime reactivators might bind wholly within the gorge itself.

5) Aromatic guidance

There has been much discussion concerning the chemical characteristics of the anionic binding site of AChE (2) as well as of ACh-binding proteins in general (7). The positive charge of ACh and of numerous potent ligands led to the designation of the site as 'anionic', and this was supported by the study of Nolte *et al.* (75) which indicated that the binding site for ACh in *Electrophorus* AChE contains 6-9 negative charges. These authors suggested that the exceptionally high on-rate observed for quaternary ligands might thus be due to the field produced by the array of negative charges. This is somewhat similar to the 'electrostatic guidance' mechanism postulated for superoxide dismutase, in which an array of positive charges

guides the negatively charged superoxide radical into the active site cavity of this rapid enzyme (76, 77).

The above hypothesis, though appealing, is at odds with our structure. We see only a small number of negative charges close to the catalytic site, but many aromatic residues both near the catalytic triad and on the walls of the narrow gorge leading down to it. The prototypic crystallographic study of a binding site for a quaternary ligand, that of the McPC603 myeloma protein, which binds phosphorylcholine selectively, showed that the quaternary moiety of the bound ligand was associated with three aromatic rings (78). Chemical modification studies of the nicotinic ACh-receptor also point to involvement of aromatic residues in its ACh-binding site (79, 80). Dougherty and Stauffer (7) have recently presented theoretical considerations, as well as experimental data obtained with model host sites, to support a preferential interaction of quaternary nitrogens with the π electrons of aromatic groups. Indeed, they present evidence that aromatic groups interact more strongly with quaternary ammonium ligands than with isosteric uncharged ligands, presumably due to the polarizability of the ion.

It is, however, pertinent to ask how the overall aromatic character of the gorge might contribute to the high rate of ligand binding and, thereby, to the high catalytic activity. First of all, it should be pointed out that the hydrophobicity of the gorge would produce a low local dielectric constant, which could result in a higher effective local charge than might be predicted from the small number of adjacent acidic groups (75). More important, the aromatic lining may permit utilization of a mechanism involving initial absorption of ACh to low-affinity sites followed by two-dimensional diffusion to the active site (81). Rosenberry and Neumann (82) earlier proposed that such a mechanism, involving multiple negatively charged sites, might explain the high on-rates for ligand-binding displayed by AChE. The aromatic lining could function analogously by providing a similar array of low-affinity binding sites (an 'aromatic guidance' mechanism). The ACh, once trapped at the top of the well, could diffuse rapidly down to the active site. This same mechanism might also provide an efficient means of achieving rapid clearance of the quaternary reaction product, choline.

B) AChE-ligand Complexes

Obviously, answers to some of the questions raised by the novel and unexpected 3-D structure of AChE can be answered by studying the 3-D structure of the native enzyme with suitable ligands. The structure of such complexes should provide direct information about the

areas of the molecule and the specific amino acid residues involved in ligand-binding and, eventually, should allow a detailed understanding of structure-function relationships which will be of pharmacological and toxicological importance.

A commonly used and convenient procedure, when applicable, for determining the structure of complexes of a given protein with ligands of interest, is to soak the ligand in question into native crystals. If the crystals survive this procedure and the ligand in question indeed penetrates to the appropriate binding site, the difference in the electron density map of the native crystal and the putative complex permits ready identification of the ligand within the binding site and elucidation of its interactions with the protein. This procedure was successfully applied to three specific AChE inhibitors of basic and pharmacological interest, and the results obtained are described in this section.

1) 3-D structure of AChE complexed with edrophonium

A crystalline complex of AChE with the drug edrophonium (EDR, Figure 11A) was obtained by soaking the ligand into native crystals of *T. californica* AChE. EDR is a powerful competitive inhibitor of AChE (17). Since EDR is quaternary, it does not penetrate cell membranes or the blood-brain barrier and thus acts primarily at peripheral sites such as the muscle endplate, and is used clinically in diagnosis of myasthenia gravis (5).

The EDR-AChE complex was obtained by soaking in 10 mM EDR for 14 days. X-ray data sets were collected as for the native crystal (40). The structure was determined by the difference Fourier technique and was refined using simulated annealing and restrained refinement in a way similar to that used for the native crystal (40) .

The overall conformations of native AChE and of the EDR complex are very similar. The quaternary nitrogen group of EDR nestles adjacent to the indole ring of Trp84, as predicted by us for the quaternary group of ACh (40), with the three alkyl groups lying in a plane approximately parallel to and ~4 Å away from that of the indole ring of Trp84 (83). Trp84 is the same residue which had been covalently labeled by the aziridinium ion (63), which is similar in structure to EDR; furthermore, EDR protects against labeling by aziridinium. Our data also demonstrate, therefore, a close correspondence between the crystal structure and that in solution. The hydroxyl group at the *meta* position in EDR is positioned between His440 $N_{\varepsilon 2}$ and O_{γ}, making hydrogen bonds of 2.9Å and 3.1Å, respectively, to these functional atoms of two of the three members of the catalytic triad (see Figure 12A). This provides a structural basis for the observation that such

meta-substituted anilinium ions are much better competitive inhibitors of AChE than either the homologous nonsubstituted anilinium ions or ones in which the ring has been substituted at a different position (17).

The most pronounced differences between the native AChE structure and that of the complex lie in the positioning of the aromatic rings of residues Phe330, close to the active site triad, and Trp279, ~17 Å away from Phe330, near the entrance of the gorge. Both residues belong to the set of highly conserved aromatic amino acids whose rings line the surface of the gorge (40). In the complex, the benzene ring of Phe330 swings from its position in the native enzyme to make a better aromatic-aromatic interaction (84) or aromatic-quaternary nitrogen interaction (85) with the ring(s) of the corresponding inhibitor (see Figure 13). As already mentioned above, a peptide containing a Phe residue homologous to Phe330 in both *Electrophorus* and *T. marmorata* AChE has been identified subsequent to photo affinity labeling (64, 65). The indole moiety of Trp279 changes its orientation even though it is located ~8 Å away from the nearest atom of either inhibitor molecule.

2) 3-D structure of AChE complexed with tacrine

A crystalline AChE complex with another drug of clinical importance was similarly obtained by soaking it into native AChE crystals. The drug, tacrine (1,2,3,4-tetrahydro-9-aminoacridine; THA, Figure 11B), is also a powerful competitive inhibitor of AChE (86). Due to its tertiary character, it can penetrate the blood-brain barrier, and is currently a promising candidate for clinical trials in the therapy of Alzheimer's disease (87).

The THA-AChE complex was obtained by soaking in a saturated solution of THA for 2 days. X-ray data sets were collected and refined in a way similar to that used for the native crystal (40). The overall conformations of native AChE and of the THA complex are very similar (83). In the THA-AChE complex, the THA moiety is stacked against Trp84, and its ring nitrogen forms a hydrogen bond with the main-chain carbonyl oxygen of His440 (3.0 Å); its amino nitrogen forms a 3.2 Å hydrogen bond to a water molecule (Figure 12B). The structure of the THA-AChE complex is thus also in agreement with earlier solution studies. Specifically, chemical labeling identified tryptophan in the active site of AChE (62, 63). Moreover, our finding that the 3-ring structure of THA is stacked opposite the indole ring of Trp84 is in full agreement with the spectroscopic observation that the competitive inhibitor, *N*-methylacridinium, which also possesses a 3-ring structure, forms a charge-transfer complex with a Trp residue in the active site of AChE in which the two ring structures face each other (20).

In the AChE-THA complex, as in the AChE-EDR complex, the differences between the native AChE structure and that of the complex lie in the positioning of the aromatic rings of residues Phe330 (Figure 13), close to the active site triad, and Trp279, ~17 Å away from Phe330, near the entrance of the gorge. The indole moiety of Trp279 changes its orientation, albeit rather differently in each complex. We cannot, at this stage, totally exclude partial occupancy at this site by a second THA molecule.

3) 3-D structure of AChE complexed with the *bis*quaternary inhibitor BW284c51

1,5-*bis*(4-allydimethylammoniumphenyl)pentan-3-one dibromide (BW284c51), is a powerful *bis*quaternary cholinesterase inhibitor (Figure 11C), which has been shown to display high selectivity for AChE relative to butyrylcholinesterase (BChE); it is, accordingly, used routinely to differentiate between the two (32). Its *bis*quaternary structure strongly suggests that while one quaternary group is interacting with the 'anionic' subsite of the active site, the other may be interacting with the 'peripheral' anionic site. Crystallographic examination of a BW284c51-AChE complex may thus permit identification of the 'peripheral' site.

A crystalline complex of AChE with BW284c51 was obtained by soaking the native crystals of *T. californica* AChE in a 1mM solution of BW284c51 in 65% saturated $(NH_4)_2SO_4$, 0.36M phosphate, pH 6.3, for 1 day at 19°C. X-ray data sets were collected as for the native crystal (40). The structure was determined by the difference Fourier technique and refined using simulated annealing and restrained refinement in a way similar to that used for the native crystal (40).

The highest positive difference electron density peaks appeared as an elongated shape with one end, near the catalytic triad, showing more density than the other, which was near the surface of the AChE molecule (Figures 14 & 15). The elongated density was fitted by the coordinates of the refined crystal structure of *r*-2,*trans*-6-diphenyl-*cis*-3-methyl-4-thianone (88) while the coordinates for the two quaternary nitrogen moieties were taken from the refined EDR-AChE structure (see above), changing the ethyl to an allyl group. The overall conformations of native AChE and of the BW-AChE complex are very similar (r.m.s. deviation ~0.42 Å). The inner quaternary nitrogen of BW284c51 nestles adjacent to the indole ring of Trp84, as had been found for the quaternary group of EDR when complexed with AChE, with the allyl chain and the two methyl groups lying in a plane approximately parallel to and ~4 Å away from that of the indole ring of Trp84. The aromatic ring of the outer quaternary group lies approximately parallel to that

of Trp279, with the quaternary nitrogen ~4.7 Å from the indole group. The keto oxygen of the inhibitor makes a rather long (3.8 Å) hydrogen bond to the hydroxyl group of Tyr121 - one of the conserved aromatic residues of the active-site gorge.

As already mentioned, the location of the inner quaternary nitrogen moiety of BW284c51, ~4 Å from Trp84, is approximately the same as that of the *mono*quaternary inhibitor, EDR, and the aromatic ring of the latter occupies roughly the same volume as that of BW284c51. In both BW-AChE and EDR-AChE the phenyl ring of Phe330 swings in a similar fashion from its position in the native structure, to make a good aromatic-quaternary nitrogen interaction (85).

It was observed much earlier, in kinetic studies employing series of *bis*quaternary compounds, that they were more powerful inhibitors than monoquaternary ligands of similar chemical character. Furthermore, in series of such compounds in which alkyl chains of increasing length separated the two charged groups (33), optimal inhibition occurred when they were separated by about 15 Å. On this basis, it was proposed that they derived their efficacy from simultaneous binding to two 'anionic' subsites. In the refined structure of BW-AChE, the distance between the two quaternary groups is 14.4 Å. Our data thus suggest that W279, and some neighboring groups at the top of the gorge, provide the second binding site for *bis*-quaternary ligands in general, including, presumably, also such *bis*quaternary oximes as HI-6 and toxogonin.

C. Conversion of AChE to BChE: Modeling and Mutagenesis

Cloning and sequencing have revealed striking sequence homology between AChE and BChE (30, 56, 89). There is 53% identity, and 73% similarity, between H-BChE and the phylogenetically distant *Torpedo* AChE (T-AChE). The three intrachain disulfides are in the same position (36, 90), and no deletions or insertions occur in the first 535 amino acids, including all those involved in catalytic activity. This marked structural similarity encouraged us to use the three-dimensional structure of T-AChE (40) to model H-BChE. We hoped, thereby, to gain an understanding of how structural differences between the two enzymes might account for known differences in specificity.

1) Model building

This was carried out interactively, using FRODO (44-46), on an Evans & Sutherland PS390 graphics system, to convert the amino acid sequence of T-AChE to that of H-BChE. The H-BChE structure was energy-minimized by the simulated-annealing program, X-PLOR (48), using the POSITIONAL refinement option.

Residues 4-534 of T-AChE can be aligned with residues 2-532 of H-BChE (56), with 53% identity and no deletions or additions (Figure 16). The catalytic triad residues are in exactly the same positions (Ser200, Glu327 and His440 in T-AChE), as are the intrachain disulfide bonds (36, 90). In the following, amino acid numbers will correspond to the numbering for T-AChE.

The starting model for H-BChE was the refined 2.8 Å X-ray structure of T-AChE (40) (Brookhaven access code 1ACE (43)). In this structure, all residues were seen, except 1-3, 485-489 and 535-537, although 81 atoms in the side-chains of some surface polar residues were not visible. To obtain the H-BChE model, all residues in the T-AChE sequence differing from those of H-BChE were changed accordingly. 356 side-chains of H-BChE are either identical to those of T-AChE or have the same number of dihedral angles. The initial H-BChE model retained the experimentally determined torsion angles for these side-chains. An additional 83 residues, with fewer side-chain torsion angles in H-BChE than in T-AChE, were also allowed to retain the experimental X-ray torsion angles of T-AChE. The dihedral angles of 87 residues with longer side-chains in H-BChE than in T-AChE were fixed to their most frequently found torsion angle values (91). In only 13 cases, where the most common rotamer of a side-chain overlapped with neighboring atoms, the second most common rotamer was taken. Energy minimization was achieved after 110 cycles of positional refinement. At that stage the C_α r.m.s. deviation between T-AChE structure and the H-BChE model was 0.28 Å. The largest shift, 1.4 Å, was displayed by Ala534Met, the last C-terminal residue seen in the X-ray structure; the second largest shift, 0.9 Å, was seen in His159Pro, a surface residue. The positions of the catalytic triad residues, Ser200, Glu327 and His440, showed only very small shifts (C_α shifts of 0.1, 0.1 and 0.14 Å, respectively).

In the T-AChE structure, the catalytic triad is located close to the bottom of a ~20 Å deep narrow cavity. This cavity was named the aromatic gorge, since about 40% of its surface area is lined with the rings of 14 aromatic amino acids (40). All these residues are fully conserved in the five vertebrate AChE sequences determined so far (56, 89), with the exception of a single case in which Phe is replaced by Tyr. This conservation suggests that these aromatic rings play

an important role in AChE function. Indeed, various lines of evidence strongly indicate that Phe330 and Trp84, which are close to the catalytic triad, may be directly involved in binding the quaternary group of ACh (see above and refs. 40, 63). The role of other aromatic residues, more distant from the active site, remains to be clarified, although we have suggested that some may facilitate access of ACh to the active site by providing low affinity binding sites both for ACh and for the choline produced by enzymic activity (40). Although as many as 30 amino acid residues contribute, to some extent, to the lining of the gorge in the experimentally determined structure of T-AChE, comparison of the sequences of T-AChE and of H-BChE, as well as of the other known AChE and BChE sequences (56), shows that only 10 amino acids, whose side-chains face the gorge, are different in BChE (Table 2). Four of these changes are unlikely to be associated with the differences in enzymic properties of the two enzymes, since they involve substitution by residues with similar side-chains, i.e., Val71Ile, Ser122Thr, Leu282Val and Ser286Thr. The other six cases **all** involve replacement of an aromatic residue in AChE by a non-aromatic residue in BChE, viz. Tyr70Asn, Tyr121Gln, Trp279Ala, Phe288Leu, Phe290Val and Phe/Tyr330Ala.

2) Substrate docking and mutagenesis of the acyl-binding pocket

We previously suggested a plausible model for the docking of ACh, in an all-*trans* configuration, within the active site of T-AChE (40). In this model, the acetyl group of ACh was positioned to make a tetrahedral bond with Ser200 O_γ. This resulted in the positively charged quaternary group of the choline moiety being within van der Waals distance (~ 3.5 Å) of Trp84, whose presence within the 'anionic' site had been earlier suggested by affinity labeling (63). This assignment was confirmed by the structures of two AChE-inhibitor complexes with the anionic-site-directed competitive inhibitors, THA and EDR (see above), as well as of the complex with the *bis*quaternary inhibitor, BW284c51. In the H-BChE model, Trp84, like the catalytic triad, does not move relative to its position in T-AChE (C_α shift of 0.07 Å). Hence it is possible to model a bound BCh molecule in the same orientation as ACh. When we thus try to dock BCh in the active site of AChE, it is clear that the bulkier butyryl moiety of BCh cannot fit into the 'esteratic' locus: it can be seen that two aromatic residues, Phe288 and Phe290, are near the modeled acetyl moiety of the bound ACh molecule (see Figure 17A). In the H-BChE model, however, substantial reduction in the size of the side-chains of the corresponding residues, Leu288 and Val290, permits the butyryl group to fit into the larger 'esteratic' pocket of the model (see Figure 17b).

The prediction of the theoretical docking procedure was tested experimentally by generating the double mutant, Phe288Leu/Phe290Val (92). Comparison of its activity towards butyryl-thiocholine and acetylthiocholine showed that it hydrolyzed the butyryl ester at a substantial rate compared to the acetyl ester, whereas no detectable activity on butyrylthiocholine was displayed by wild-type T-AChE. The double mutant was also inhibited well by the BChE-specific organophosphate inhibitor, isoOMPA, whereas the wild type *Torpedo* enzyme was almost totally resistant to this reagent (Figure 18).

3) Modeling and mutagenesis of the peripheral anionic site

Two other changes which involve substitution of aromatic by nonaromatic residues, are of amino acids whose aromatic side-chains undergo localized conformational changes upon binding of the competitive inhibitors, THA and EDR, as shown by our crystallographic data (see above). These changes are in Trp279 and Phe330. Phe330 is close to the ligand-binding site, and in both complexes, the conformational change observed involves an aromatic-aromatic or an aromatic-quaternary nitrogen interaction with the bound ligand (85). Trp279 is, however, at least 8 Å away from the 'anionic' site, and any direct contact with a small inhibitor bound at the 'anionic' site can be precluded. Is Trp279, which undergoes a conformational change upon binding of inhibitors to T-AChE, part of a different site? *Bis*quaternary ligands, such as decamethonium (24), are more potent inhibitors of AChE than the corresponding *mono*quaternary ligands, and this has been ascribed to their binding simultaneously to the 'anionic' subsite of the catalytic site and to the 'peripheral' anionic site (33). Binding studies of several series of *n*-alkyl *bis* ammonium ions have shown an optimal separation of 14-15 Å between the two quaternary groups, while the distance between the two indole moieties of Trp84 and Trp279 is ~15 Å in AChE. These data can be rationalized by assuming that Trp279, at the mouth of the active-site gorge, is an important component of the 'peripheral' anionic site. The X-ray structure of the complex of T-AChE with the potent AChE-selective *bis*quaternary anticholinesterase agent, BW284c51 (32), clearly implicates Trp279 in the binding site for the distal quaternary group (see above). The enhanced potency of *bis*quaternary compounds, relative to the corresponding *mono*-quaternary ligands, does not hold for BChE (33). Replacement of Trp279 by Ala in BChE might thus explain its lack of a 'peripheral' site, and its failure to display enhanced sensitivity to *bis*-quaternary inhibitors. The mutation Trp279Ala of *Torpedo* AChE was designed to test the above hypothesis (92). Inhibition of Trp279Ala by the 'peripheral' site ligand, propidium (25), was reduced at least 10-fold relative to inhibition of wild-type T-AChE by this ligand, whereas inhibition by EDR, which is directed towards the 'anionic' subsite of the active site, was not

affected (Figure 19). Inhibition of the Trp279Ala mutant by BW284c51 was only two-fold less than that of wild-type T-AChE. It must be remembered that this *bis*quaternary ligand is still capable of reacting with the 'anionic' subsite as in the wild-type enzyme; furthermore, our model building reveals that several residues other than W279 may contribute to the 'peripheral' site, and may participate to differing extents for different ligands. These residues include Tyr70, Tyr121 and Asp72. Additional model-building and data collection on suitable AChE-ligand complexes will be necessary in order to fully delineate the 'peripheral' site.

IV) DISCUSSION & CONCLUSIONS

In the research covered by this final report, we have described, for the first time, the elucidation of the three-dimensional structure of acetylcholinesterase (AChE), that from *Torpedo californica*, the purification and crystallization of which we had reported previously (38, 93). We have further described the structure of complexes of the enzyme with three potent and characteristic competitive inhibitors of basic and pharmacological interest. Finally, we have shown that, due to their high sequence homology and similarity, it is possible to successfully model human BChE (H-BChE) on the basis of the three-dimensional structure of *Torpedo* AChE. The data so obtained can then be used, in combination with 'state-of-the art' site-directed mutagenesis technology, so as to modify the specificity of the wild-type AChE with a high degree of control and precision, and thereby to confer on it characteristic features of BChE. This powerful 'modeling-and-mutagenesis' approach should obviously be of general validity for implementation on AChE and BChE from other sources.

The three-dimensional structure of AChE was revealed as a novel and unexpected structure, in which the active site was found to be located near the bottom of a deep and narrow cavity, which we named the 'aromatic gorge', since it was lined with the rings of 14 highly conserved aromatic amino acid residues. The subsequent structural studies of the ligand-AChE complexes, as well as the modeling and the site-directed mutagenesis studies, have permitted an initial understanding of the functional significance of the structure, and allowed us to ascribe a specific role to some of the amino acid residues in the gorge.

AChE was revealed to be a typical serine hydrolase, inasmuch as it contains a catalytic triad, composed of residues Ser200, His440 and Glu327; but the occurrence of Glu in the triad is a novel feature, and AChE indeed belongs to a new family of enzymes, the α/β hydrolase family, which gathers together a repertoire of enzymes which share a common fold but differ widely in phylogenetic origin and specificity (94).

AChE differs, however, from serine hydrolases described previously in the fact that its active site is located near the bottom of the 'aromatic gorge', the novel and unique structural feature already mentioned. Although the specific subsite for the quaternary head group of the substrate, acetylcholine (ACh), had always been believed to be an 'anionic' site composed of a number of negative charges, and physicochemical evidence had been provided in support of this possibility (75), modeling of ACh within the aromatic gorge strongly indicated that the quaternary group was interacting with the indole ring of a specific conserved tryptophan residue, Trp84, which

independent chemical evidence had recently implicated in the binding site (63). This unexpected assignment was fully borne out by the direct experimental evidence provided by the studies with the complexes of AChE with the two quaternary ligands, EDR and BW284c51, in both of which the quaternary group clearly pointed directly at the indole ring of Trp84. Furthermore, the fused ring structure of the tertiary ligand, tacrine, quite clearly oriented itself parallel to the same indole ring, confirming the much earlier prediction made for a homologous ligand, *N*-methylacridinium, on the basis of fluorescence spectroscopy (20).

The crystallographic data on the ligand-AChE complexes revealed, also, interaction of the bound ligand with the ring of a second member of the set of conserved aromatic residues in the gorge, namely Phe330. Whereas the position of the indole ring of Trp84 did not move significantly upon ligand-binding, the phenyl ring of Phe330 moved significantly, ~45° for EDR and BW284c51, and 90° in the case of tacrine, where it lined up parallel both to the indole and to the three-ring structure of the bound ligand. In this case, too, independent evidence, obtained in solution by use of a photo affinity labeling probe, confirmed the crystallographic assignment (65).

The involvement of aromatic rings in the so-called 'anionic' site was unexpected *a priori*, but in addition to the good agreement with the labeling studies in solution, which were mentioned above, the participation of aromatic rings in interaction with quaternary groups in general received support from a recent study which invoked both theoretical considerations and the use of model host compounds. The chemical basis for such interactions appears to be a charge-charge interaction between the quaternary group and the π electrons of the aromatic ring (7). Similar interactions occur also in the phosphorylcholine-binding site of the MoPc603 antibody (95) and in the ACh-binding site of the nicotinic acetylcholine receptor (80, 96), and conformational changes involving aromatic groups have been invoked as playing a role in ligand-gated channels (97). The literature relating to quaternary-aromatic interactions has been reviewed recently (98).

The crystallographic studies on the ligand-AChE complexes assigned a role to 2 of the 14 aromatic residues in the gorge, those directly involved in interaction with the quaternary group of ACh. One possible role for aromatic residues more distal from the active site, i.e., further up the gorge, would be to provide low affinity binding sites for the substrate molecule which would facilitate its movement down the gorge towards the active site. We have coined this putative role 'aromatic guidance' (40) by analogy with the 'electrostatic guidance' invoked earlier to explain the high efficacy of superoxide dismutase (77). This suggestion may partially or fully explain

the role of some of the aromatic residues in the gorge, but the modeling of H-BChE, on the basis of T-AChE, taken in conjunction with the site-directed mutagenesis assigns more specific roles to others. Thus inspection of the T-AChE structure indicated that the rings of the two phenylalanine residues, Phe288 and Phe290, provide a binding pocket for the acetyl moiety of ACh, and that their dimensions precluded the entrance of the butyryl moiety into this pocket, thus providing an explanation at the molecular level for the known specificity of AChE. Similar inspection of the H-BChE model suggested that replacement of these two aromatic residues, which are conserved in AChE, by Leu and Val residues in BChE, permits this latter enzyme to accommodate the butyryl group in the corresponding binding pocket, thus allowing it to display broader specificity. The site-directed mutagenesis experiments, involving production and characterization of the Phe288Leu/Phe290Val double mutant, provided clear-cut support for the structural assignments and for the modeling.

Comparison of the three-dimensional structures of the native enzyme with that of the EDR and tacrine complexes indicated that ligand binding was not accompanied by any overall change in protein conformation. There was, however, in addition to the major movement of the aromatic ring of Phe330 already noted, substantial movement of the indole ring of Trp279, even though it was not in direct contact with the bound ligand. The position of this residue, at the top of the gorge, ~15 Å from the 'anionic' site, suggested that it might be part of the 'peripheral' anionic site. Indeed, various lines of evidence converge to substantiate this assignment. Most important, the three-dimensional structure of the AChE-BW complex reveals the distal quaternary group to be near the indole ring of Trp279, and it is commonly accepted that such *bis*quaternary compounds derive their enhanced potency from their ability to span the two 'anionic' sites (33). Furthermore, it is known that this enhanced potency does not extend itself to BChE, which thus appears to be lacking the 'peripheral' site (33). It was, therefore, significant that BChE is also devoid of W279, even though this residue is conserved in the AChE sequences studied so far. Site-directed mutagenesis provided further support for the involvement of W279 in the 'peripheral' anionic site, since characterization of the Trp279Ala mutant of *Torpedo* AChE showed that its inhibition by the characteristic peripheral ligand, propidium, was greatly reduced relative to inhibition of the wild-type enzyme, whereas inhibition by EDR, which is directed to the 'anionic' subsite of the active site, was not affected by the mutation. Thus, the mutagenesis data, as well, support the participation of Trp279 in the 'peripheral' anionic site.

The data amassed so far assign specific roles to only five of the fourteen amino acids in the aromatic gorge, and the function of the remaining nine has still to be clarified, as has that of other residues in the gorge. At least two tyrosine residues, Tyr70 and Tyr121, in the upper part of the

gorge, are near Trp279, and it will be necessary to examine carefully the structure of the AChE-BW complex, as well as similar complexes with 'peripheral' site ligands such as propidium, and to study suitable mutant forms of the enzyme, in order to assess whether they indeed participate directly in the 'peripheral' site. The same holds true for the acidic residue, Asp72.

In summary it can fairly be stated that the studies carried out in the framework of the present contract, and summarized in the present report, have greatly increased our understanding of the specificity and mode of action of AChE. Many important features, however, remain open issues which await resolution, and may help us to understand fully the structural basis for its remarkable catalytic activity and for its rapid inhibition by certain organophosphates.

Table 1. Crystallographic data

X-ray data sets were collected at room temperature for a native crystal and for the two heavy atom derivatives, using a Siemens/Xentronics area detector installed on a Rigaku rotating anode generator operating at 40 kV, 250 mA with a graphite monochromator. In addition, a native data set, collected at 0° C, was used for refinement. Each data set was collected from a single crystal. Data frames of 0.25°, with an exposure time of 70 s, were collected and processed with the XENGEN (99) and XDS (100) software packages. All subsequent crystallographic calculations were performed using the CCP4 computing package (from the Daresbury laboratory, UK) including the Dickerson-type refinement for heavy atom parameters as implemented in the program PHASE (101). The anomalous differences of both the uranyl and the mercury derivative were included in the phasing.

Space group: $P3_121$ (a=110 Å, c=135 Å at RT#; a=b=113 Å, c=137 Å at 0°C), 1 monomer/asymmetric unit				
Derivative	Native (0°C)	Native (RT)	$UO_2(NO_3)_2$ (RT)	$HgAc_2$ (RT)
Number of Measurements	83,667	41,463	44,736	43,413
Number of unique reflections (completeness %)	23,587 (90)	22,523 (89)	23,631 (93)	24,297 (96)
Resol. limit (Å)§	2.8	2.8	2.8	2.8
R_{sym} (%)*	10.4	10.3	11.5	11.1
R_{iso} (%)†			17.7	15.1
MIR phasing in resol. range 15-2.8 Å				
R_{Cullis} (%)‡			43.9	65.4
rms f_H/E_{iso} (all reflections/highest resol/ range)			3.16/3.00	1.35/1.56
rms f''_{calc}/E_{ano} (all reflections/highest resol. range)			0.71/0.40	0.25/0.25
Number of sites			6	4
Mean figure of merit (MIR)	0.59 all reflections/0.32 the highest resol. shell			
Mean figure of merit (after solvent flattening)	0.80 all reflections/0.68 the highest resol. shell			
Mean phase change MIR vs solvent flattening	32° all reflections/53° the highest resol. shell			

#RT=Room temperature (~20°C)
§Resol. = Resolution
*$R_{sym} = \Sigma|I - \langle I\rangle|/\Sigma\langle I\rangle$
†$R_{iso} = \Sigma\{||F_{PH}| - |F_P||\}/\Sigma|F_P|$
‡$R_{Cullis} = \{\Sigma||F_{PH} \pm F_P| - F_{H(calc)}|\} / \{\Sigma|F_{PH} - F_P|\}$ for centric reflections.

Table 2. Residues with side-chains facing the active site gorge where differences are found between AChEs and BChEs

	AChE				BChE		
Res.	T	H	M	B	H	M	R
70	Y	Y	Y	Y	N	N	N
71	V	V	V	V	I	I	I
121	Y	Y	Y	Y	Q	Q	Q
122	S	S	S	S	T	T	T
279	W	W	W	W	A	R	V
282	L	L	L	L	V	L	V
286	S	S	S	H	T	S	S
288	F	F	F	F	L	L	L
290	F	F	F	F	V	I	V
330	F	Y	Y	Y	A	A	A

T - *Torpedo*, H- Human, M-Mouse, B-Bovine, R-Rabbit

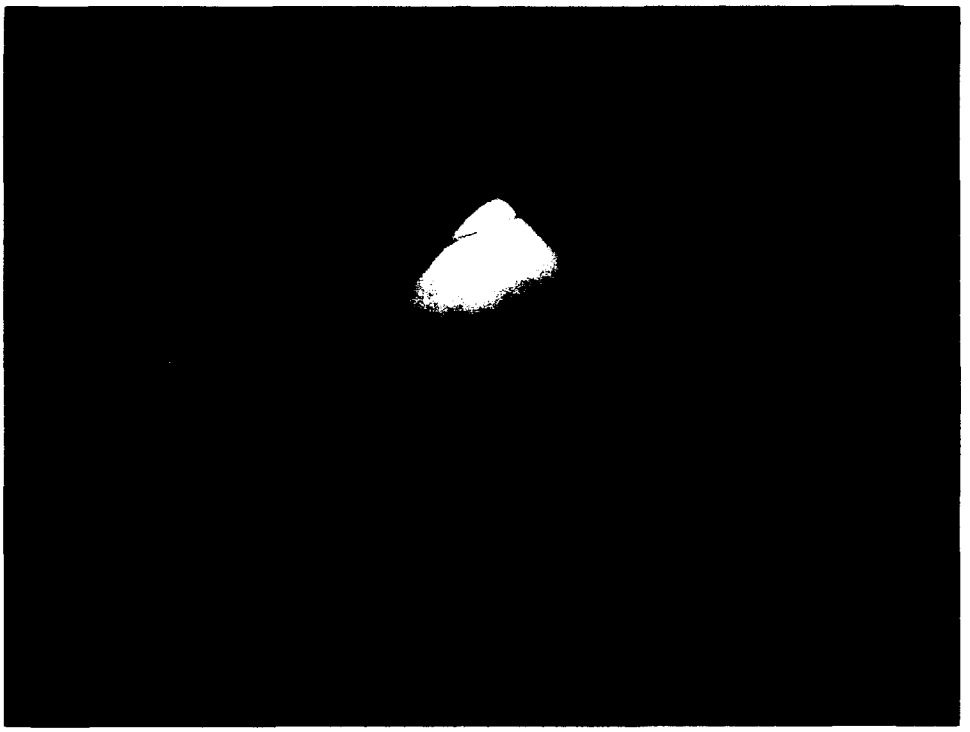

(A)

(B)

Figure 1. Crystals of AChE from *Torpedo californica* obtained by precipitation from **(A)** PEG200 and **(B)** concentrated ammonium sulfate. In both cases the crystals shown are longer than 0.5 mm in their shortest dimension.

Figure 2. A single frame image obtained for a native crystal of *Torpedo* AChE (obtained from ammonium sulfate) on a Siemens/Xentronics area detector at room temperature, exposure time, 120 s; oscillation, 0.25°; crystal-detector-distance 12 cm; $2\theta = 10°$.

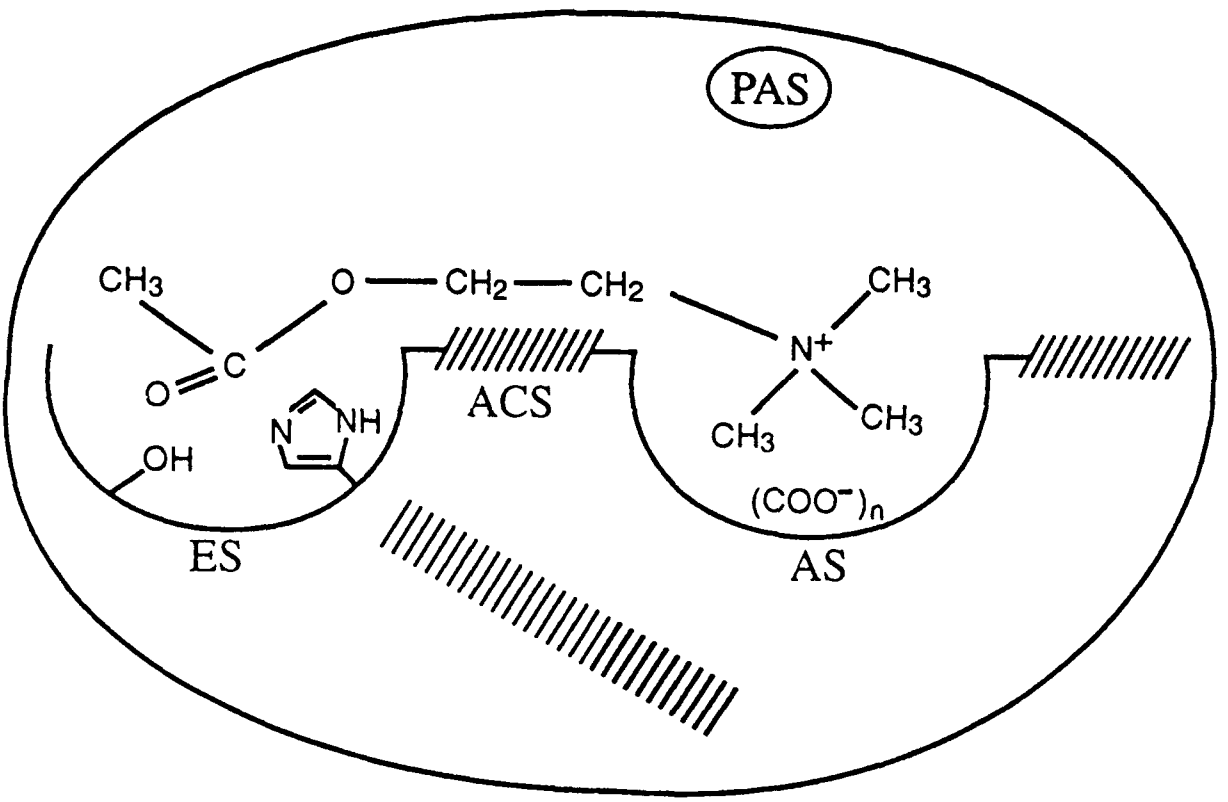

Figure 3. Schematic representation of the binding sites of AChE based upon previous kinetic, spectroscopic and chemical modification studies. **ES** - esteratic site; **AS** - 'anionic' substrate binding site; **ACS** - active-site-selective aromatic cation binding site; **PAS** - peripheral anionic binding site(s). The hatched areas represent putative hydrophobic binding regions. The ACh molecule is shown spanning the esteratic and anionic sites of the catalytic center. Imidazole and hydroxyl side-chains of His and Ser are shown within the esteratic site. $(COO\text{-})_n$, within the anionic site, represents 6-9 putative negative charges.

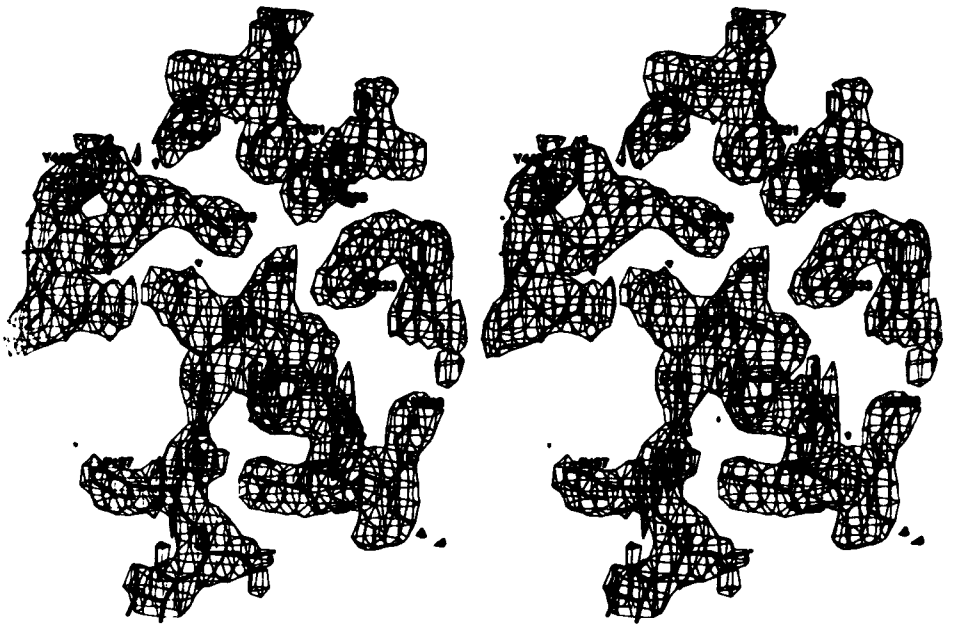

Figure 4. Representative portion, displayed in stereo, of the MIR-WANG 2.8 Å electron density map of AChE, in the vicinity of the active site. The final refined atomic model is superimposed. The O_γ of Ser200 is seen to lie at the elbow of the strand-turn-helix motif, within hydrogen bonding distance of His440. Glu327, the third member of the catalytic triad, cannot be seen since it is out of the plane of the figure. Note the large number of aromatic residues in the immediate vicinity of the active-site serine.

Figure 5. (A) Stereo C_α trace of the AChE monomer looking into the active site gorge. Residues in the catalytic triad are indicated by solid black lines. (B) Stereo ribbon diagram made using the RIBBON program (102), oriented as in Figure 5A. The N-terminus is located at the top right of the picture, and the C-terminus at the lower left. The 12-stranded β-sheet is approximately parallel to the plane of the figure, with its convex surface pointing up. The sheet is sandwiched between six helices, two on its concave surface (underneath in this view) and four on its convex surface. The other eight helices all occur in loops above the sandwich. (C) Secondary structure cartoon showing the topology of AChE, with the β-sheets represented by grey arrows and the α-helices by rods. The dashed vertical lines indicate that the central eight-stranded mixed β-sheet makes relatively few hydrogen bonds to either the first or the last β-hairpin loops. The numbering of the central β-sheet corresponds to that of the 8-stranded β-structure of α/β hydrolase fold (94). Several helical stretches are found between strands 6-7 and 7-8 (see Figure 6); for the sake of clarity only the last helix is displayed in each case. The filled circles indicate the positions of the catalytic triad; Ser200 occurs after strand 5, Glu327 after strand 7, and His440 after strand 8.

T. californica Acetylcholinesterase

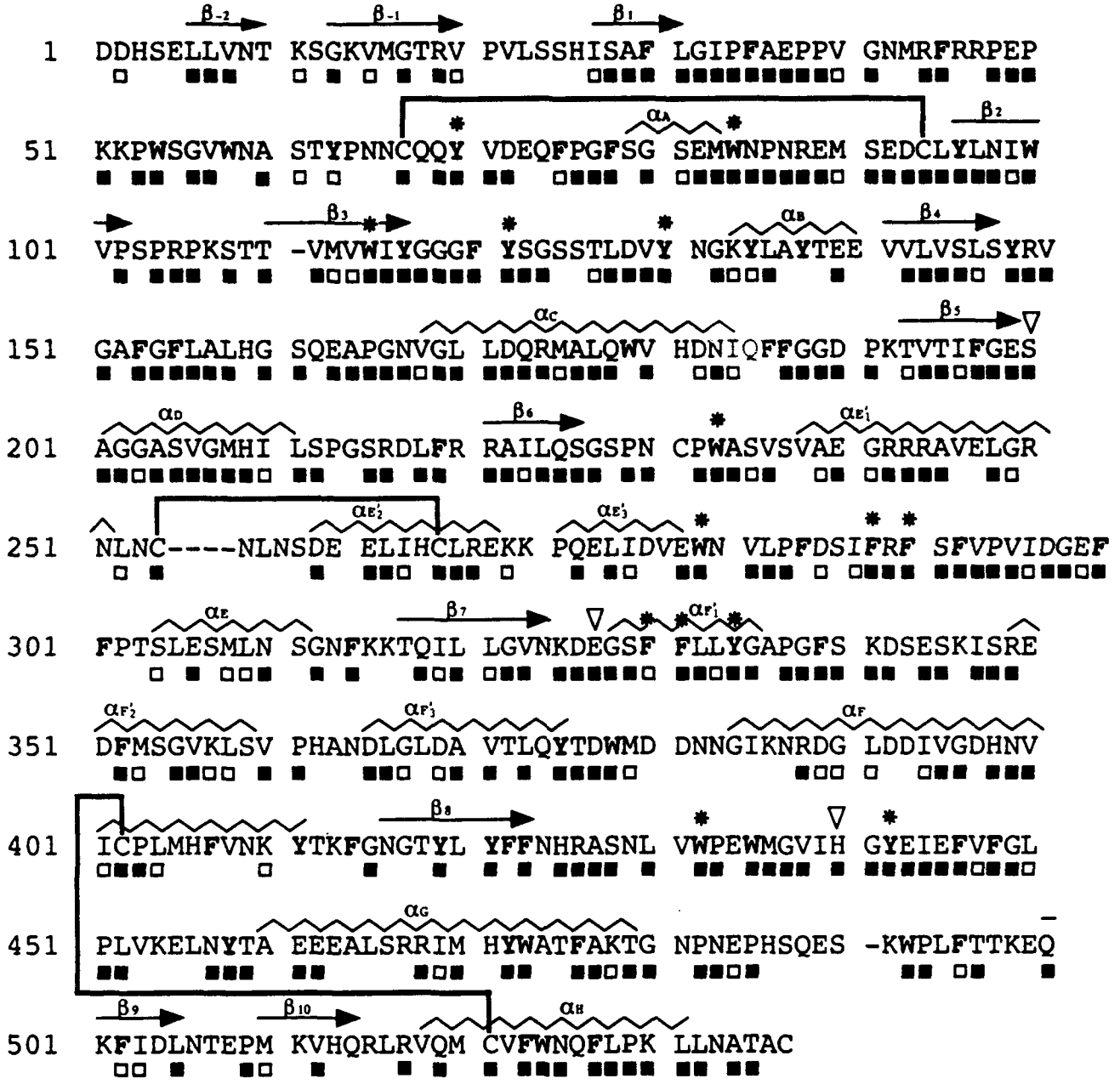

Figure 6. Amino acid sequence and secondary structure of the polypeptide chain of PI-anchored AChE from *T. californica* (taken from (15, 35, 42)). Aromatic residues are in bold, with those whose side-chain faces the active site pocket being starred (*). The members of the catalytic triad are marked with an open arrowhead. Sequence homology was examined between this AChE and four others (*T. marmorata*, mouse, human and bovine (55)). Dashes indicate gaps in the *Torpedo* sequence relative to the mammalian sequences. All identical residues, i.e. conserved in all five sequences, are marked by □. Similar residues are marked by □, where similarity is considered to be present if G is replaced by A (or vice versa), T by S, D by E, K by R and L by V, I or M. The pairs of cysteines in the conserved disulfide bridges (36) are connected appropriately. β-stands and α-helical regions are indicated by arrows and by zig-zag lines, respectively, above the amino acid sequence.

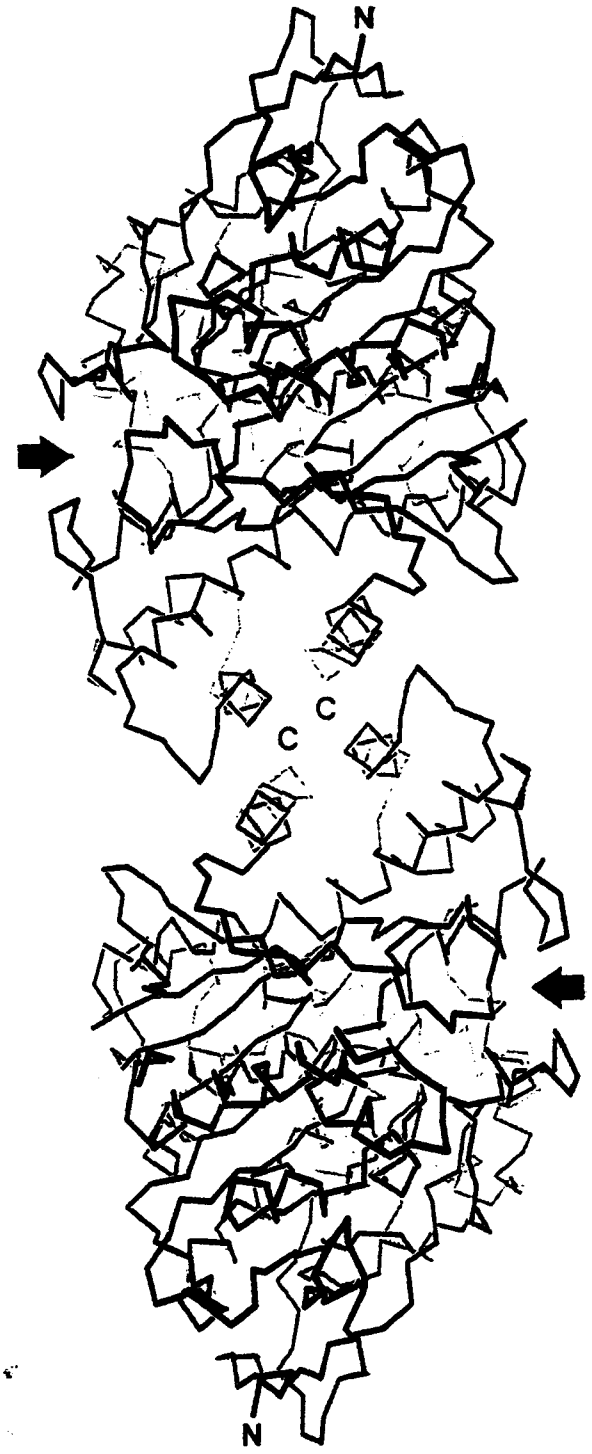

Figure 7. C_α trace of an AChE dimer, viewed down the crystallographic two-fold axis. The active sites, whose positions are indicated by arrows, are about 60 Å apart. A four-helix bundle composed of α-helices F3 and H from each subunit and a short loop between α-helices F3 and F are the only observed non-covalent contacts between the two subunits.

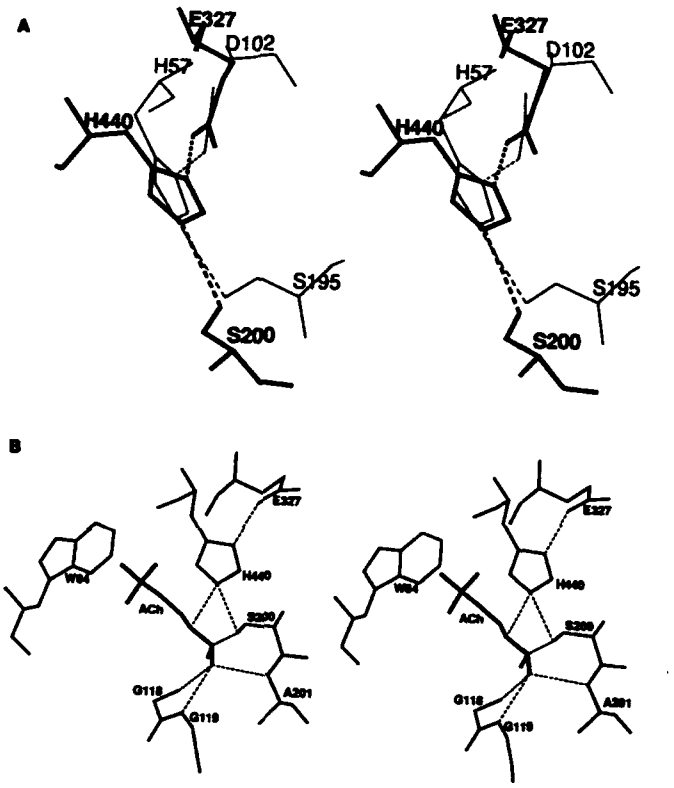

(A)

(B)

Figure 8. (A) Superposition of the catalytic triads of AChE (Ser200-His440-Glu327) (darker) and Cht (103) (Ser195-His57-Asp102) (lighter) showing that the main chains point in opposite directions at the histidine and the serine when the imidazole rings of the histidines are superimposed. The hydrogen bonds of the active site triads are marked by dashed lines. The distance Ser200O_γ - His440$N_{\varepsilon 2}$ is 3.1 Å; His440$N_{\delta 1}$ - Glu327$O_{\varepsilon 1}$ is 2.5 Å. (B) A theoretical model for the docking of ACh onto AChE. The triad and the nearby environment are shown, including the oxyanion hole and Trp84. The thin solid line marks the bond produced in the transition state between Ser200O_γ of AChE and the carbonyl carbon of ACh. Dashed lines indicate the putative hydrogen bonds.

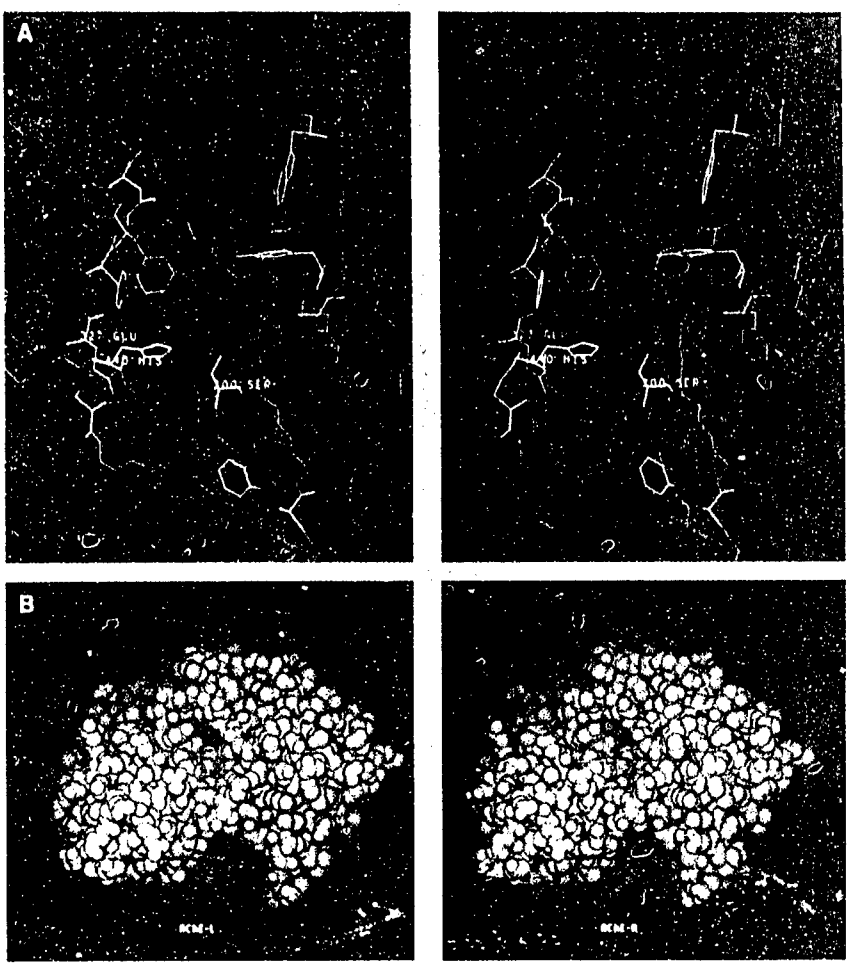

(A)

(B)

Figure 9. (A) Stereo illustration of a thin slice through the AChE monomer. The blue dot van der Waals surface shows the narrow gorge leading down to the active site. The backbone is pink, the aromatic groups are light green, and the catalytic triad is white. (B) Space-filling stereo view of the AChE molecule looking down into the active site gorge using the MacImdad program. Aromatic residues are green and other residues grey. Ser200 (red) and Glu199 (cyan) are visible towards the bottom of the gorge.

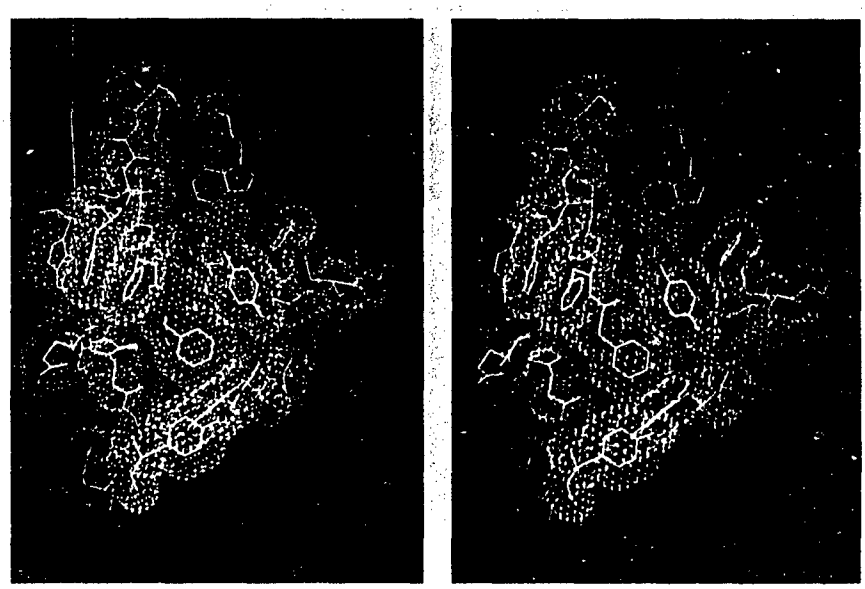

Figure 10. Stereo representation which includes all residues contributing to the active site gorge. The view is rotated ~90° around the vertical axis relative to the view shown in Figure 9A. Aromatic residues are colored gold and other residues blue, both types being embellished with van der Waals dot surfaces. The catalytic triad residues are pink. This view of the gorge clearly shows that the rim on one side is much higher than on the other.

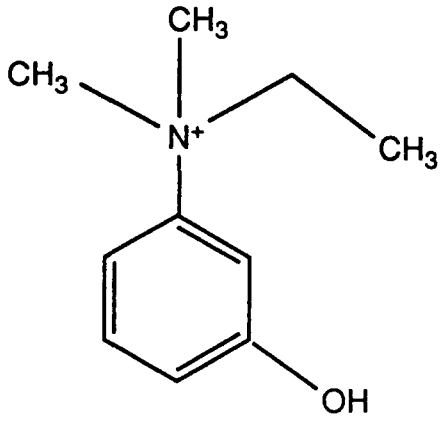

a

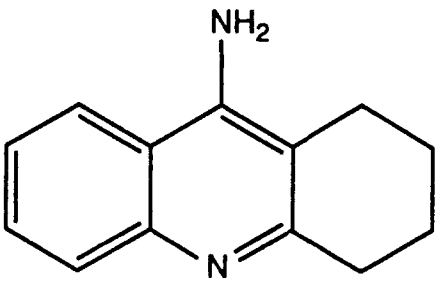

b

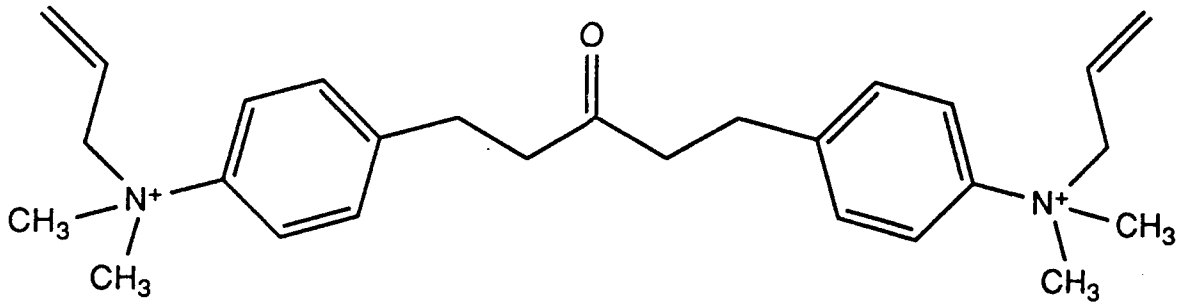

c

Figure 11. Chemical formulae of the anticholinesterase agents: (A) EDR; (B) THA; (C) BW284c51.

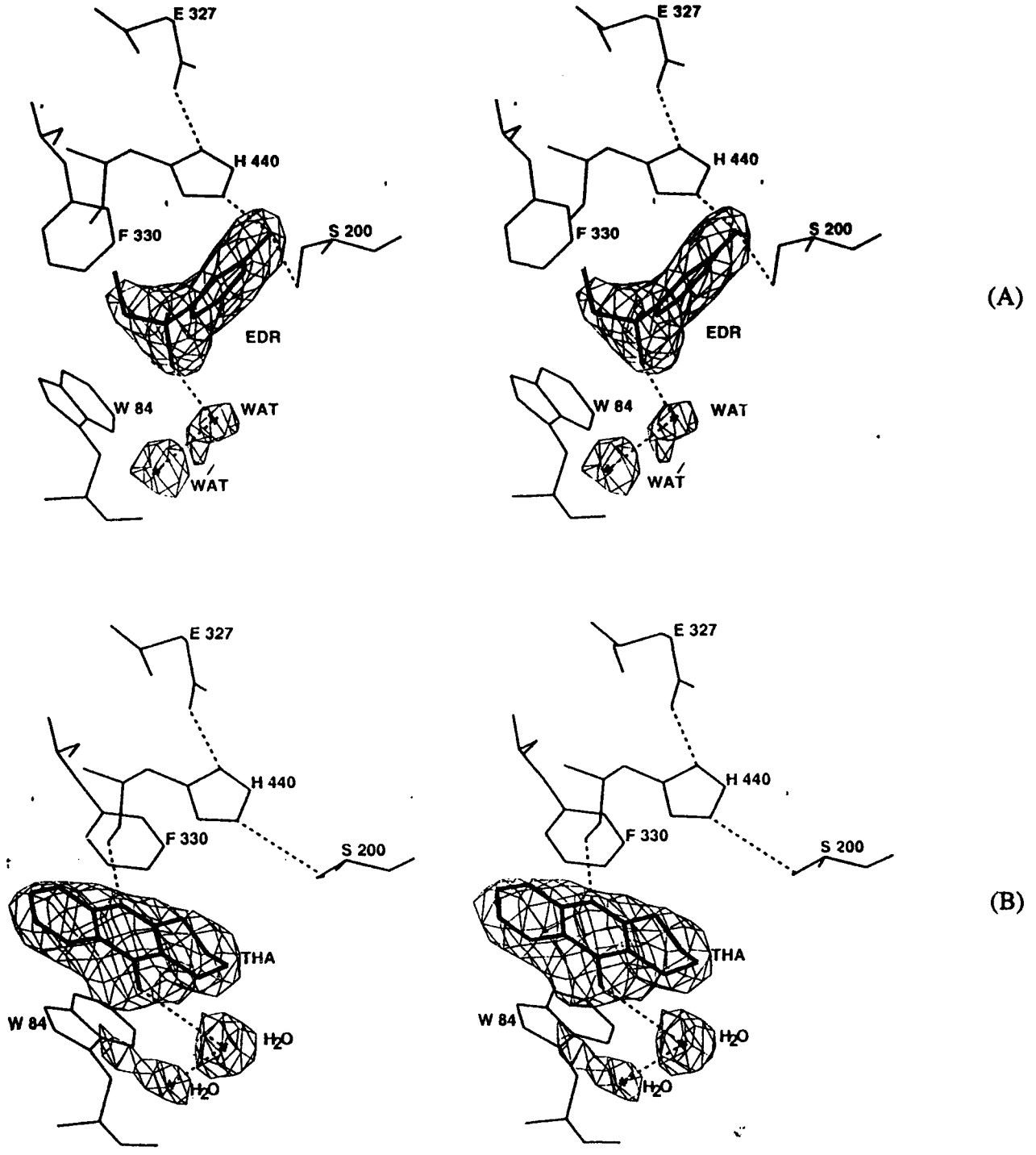

Figure 12. (**A**) Initial stereo (F_{obs}-F_{calc}) electron density map at 2.8 Å resolution of (**A**) the EDR-AChE complex, (**B**) the THA-AChE complex, each contoured at 3.9 σ, after refinement of the native protein coordinates in the absence of ligand. The final refined coordinates (R=18.2% and 18.4% for the EDR-AChE and THA-AChE complexes respectively) of the protein-ligand complexes are superimposed on each maps.

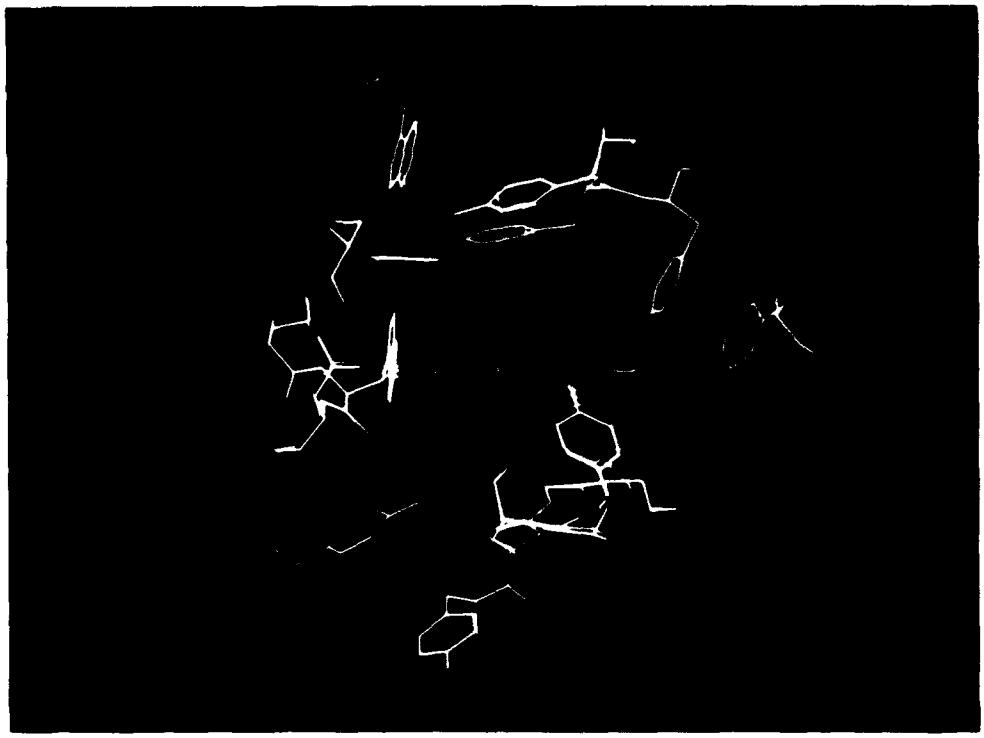

(A)

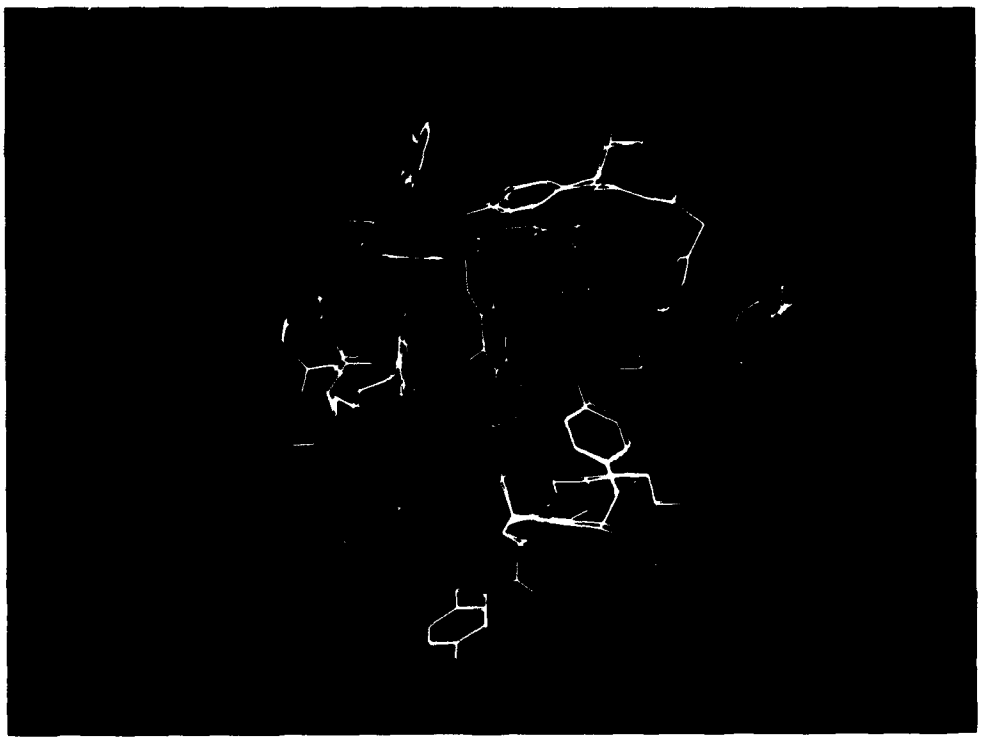

(B)

Figure 13. Comparison of the refined crystal structures of native AChE versus (**A**) the EDR-AChE complex, and (**B**) the THA-AChE complex in the vicinity of the active site, with key amino acids labeled and the bound ligands designated as residue 550. The native structure is shown in yellow in both complexes. The EDR-AChE complex is shown in pink and the THA-AChE complex in blue. Note that in both complexes the phenyl ring of F330 is the only moiety in the protein which moves significantly, relative to the native structure, upon ligand binding.

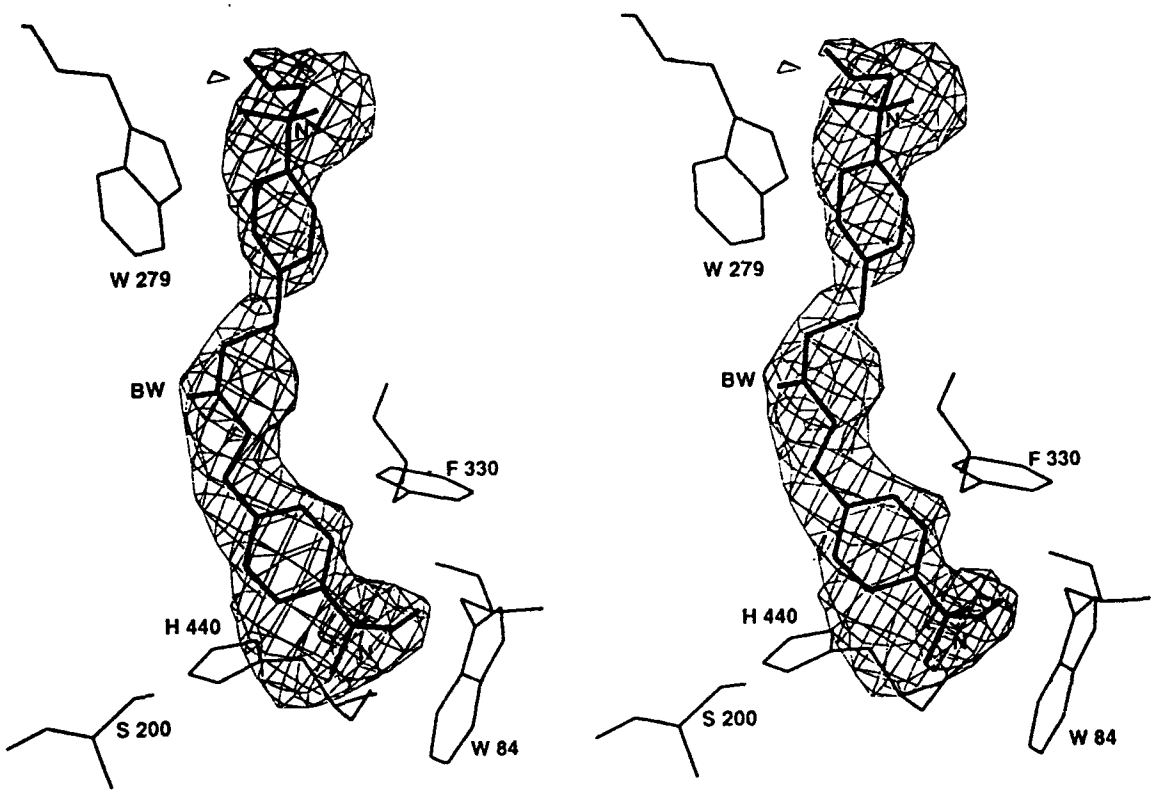

Figure 14. Initial stereo (F_{obs}-F_{calc}) electron density map at 2.8 Å resolution of the BW-AChE complex, contoured at 3.5 σ, after refinement of the native protein coordinates in the absence of ligand. The final refined coordinates (R=19.8%) of the protein-BW complex are superimposed on this map.

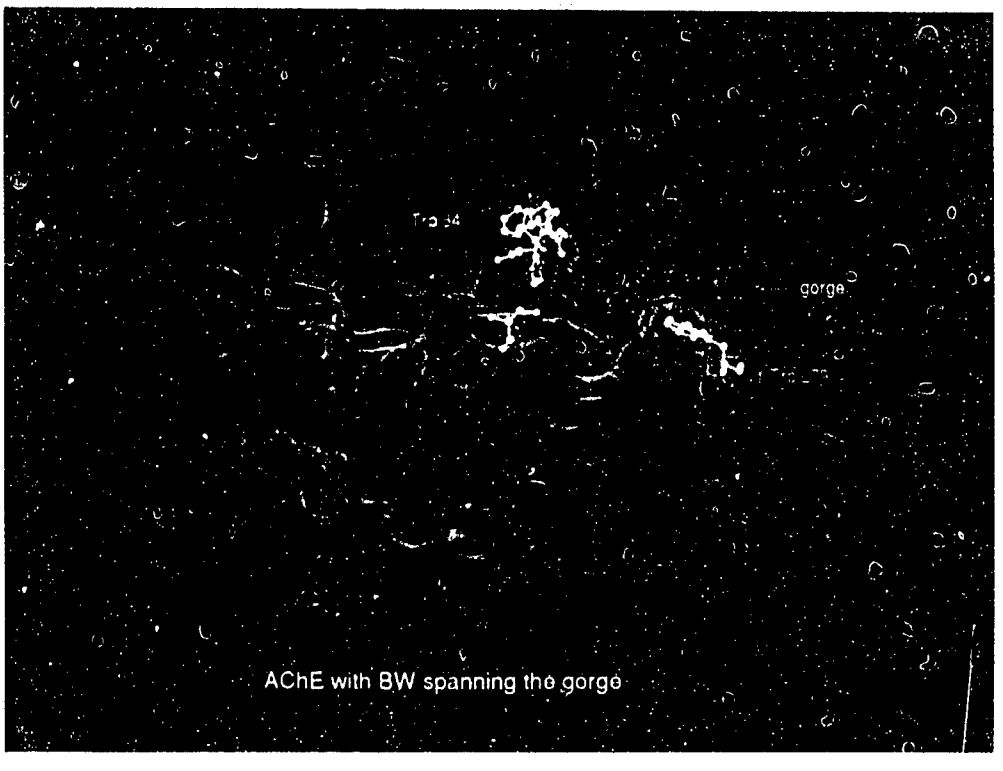

Figure 15. A cross section of the active site gorge, based on the X-ray structure of the AChE-BW complex, shows BW284c51 lying along the length of the gorge, with its two quaternary groups close to Trp84 and Trp279.

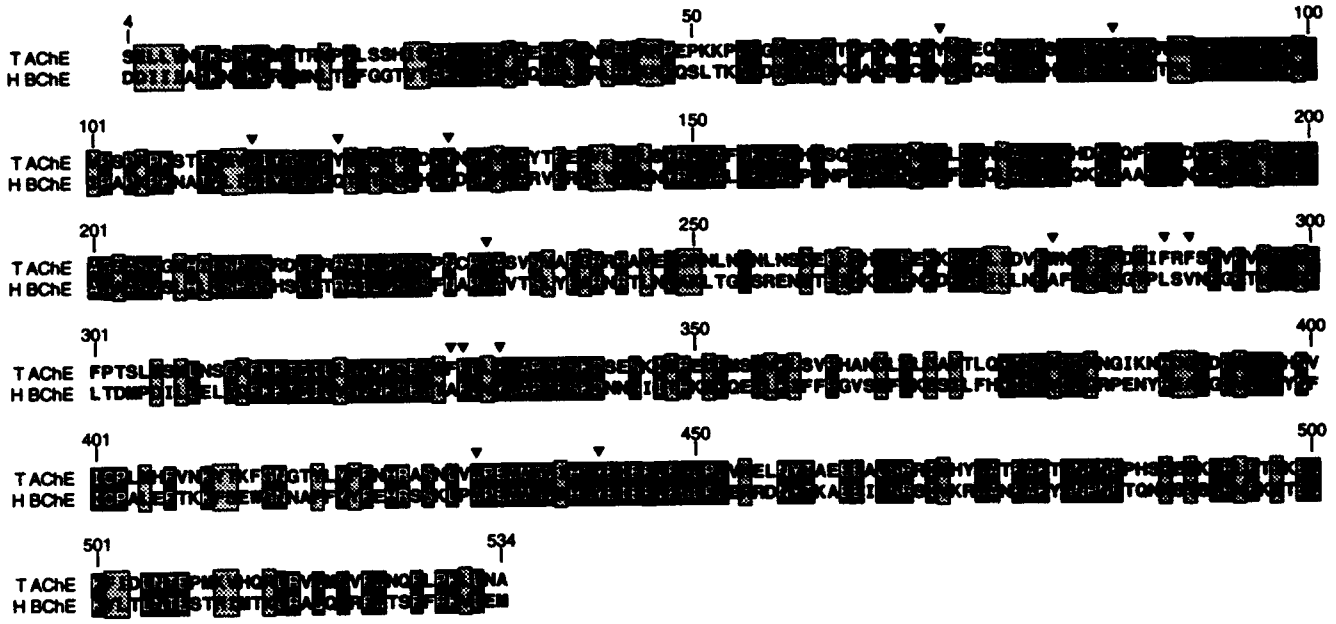

Figure 16. Comparison of the amino acid sequences of *Torpedo californica* AChE and human BChE. Residues 4-534, which are seen in the X-ray structure of the *Torpedo* structure are compared. Reverse video indicates identical residues, whereas grey boxes indicate similar residues (i.e. A and G; T and S; D and E; K and R; F and Y; N and Q; L, V, I and M). Aromatic residues in the active-site gorge are marked with ∇. Numbering is that of *Torpedo* AChE.

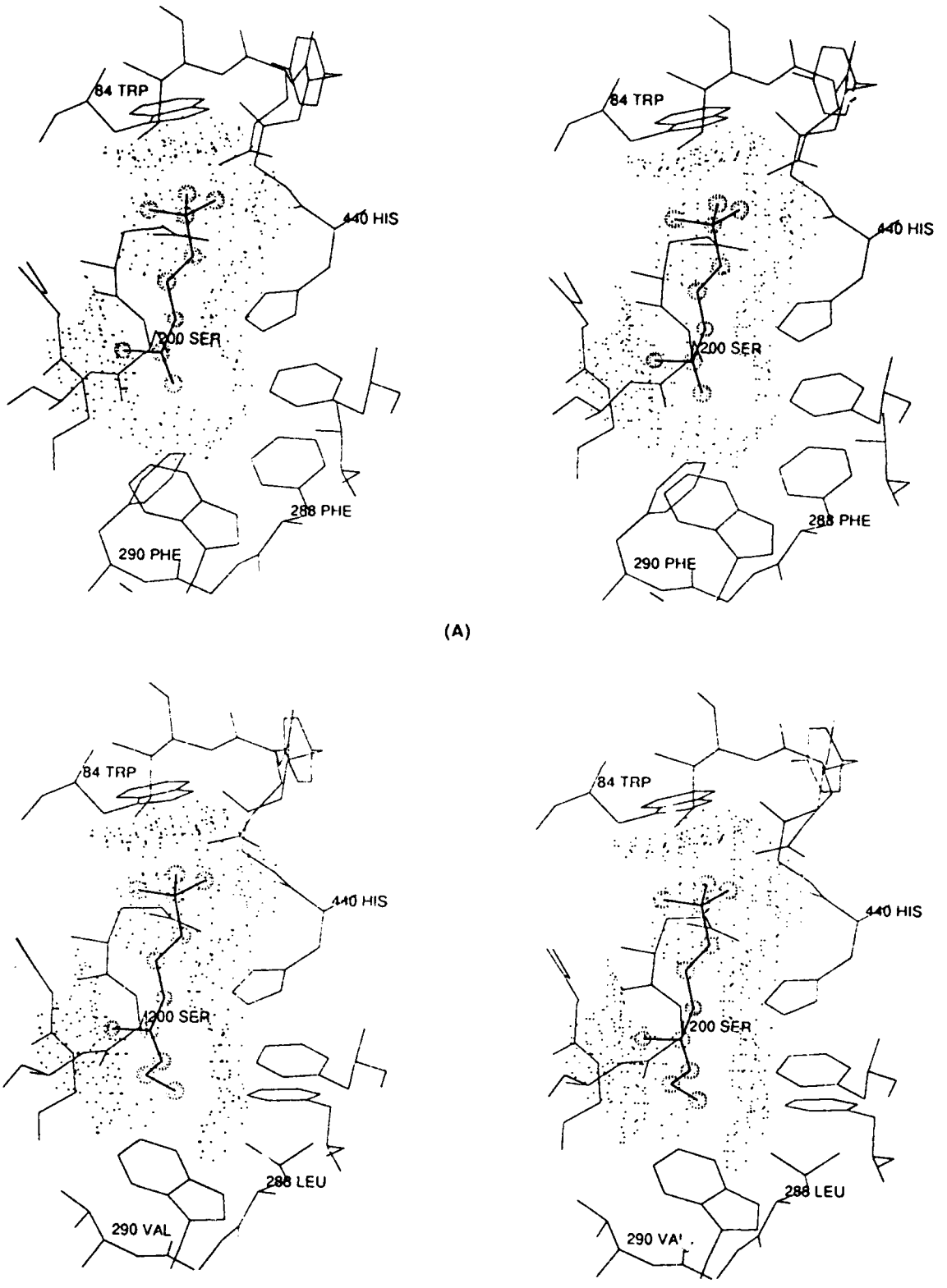

Figure 17. (a) Stereo view of the van der Waals surface of atoms within 3 Å of ACh in the *Torpedo* AChE X-ray structure. (b) Stereo view of the van der Waals surface of atoms within 3 Å of BCh in the human BChE model.

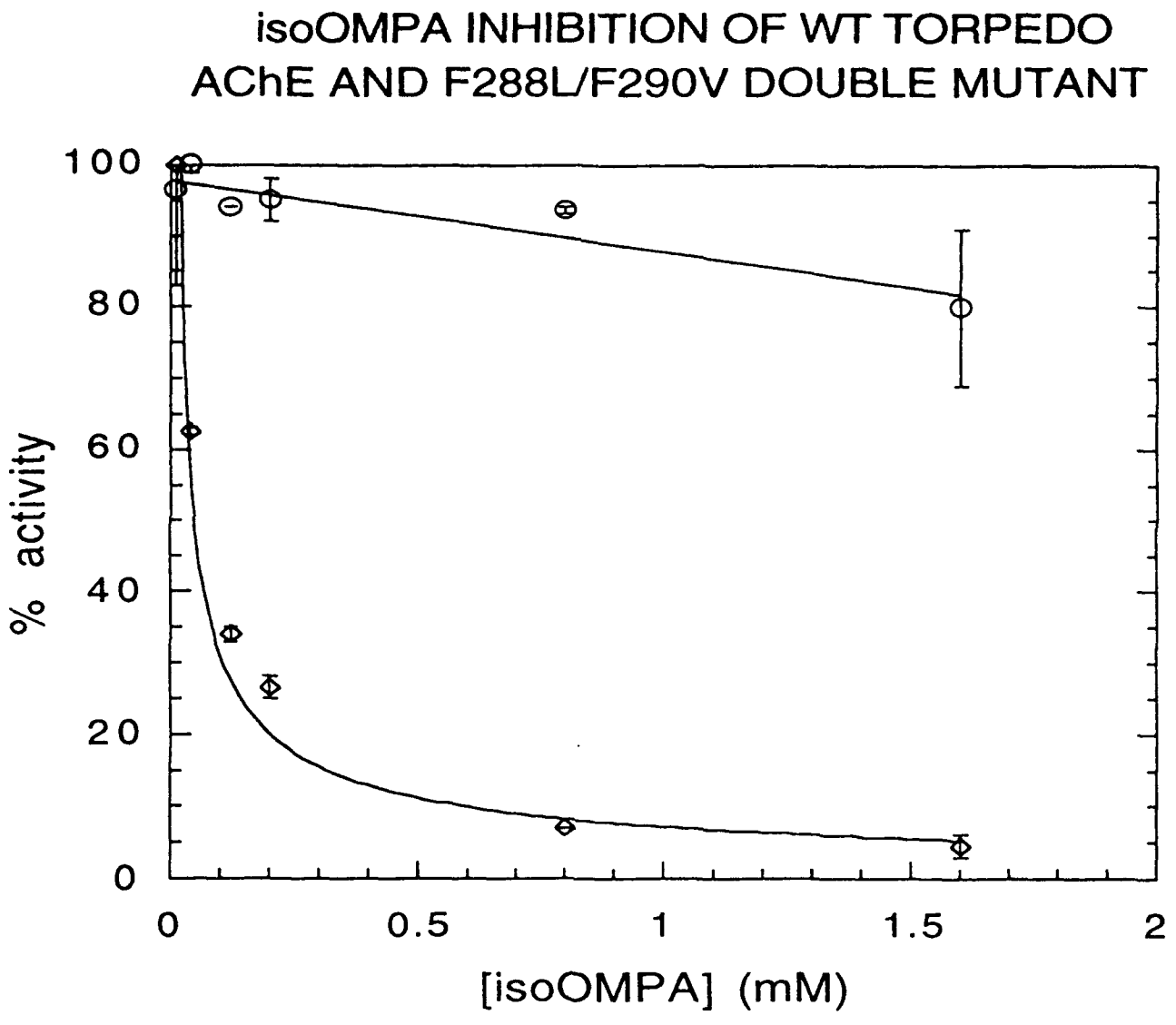

Figure 18. Concentration-dependence of inhibition by isoOMPA of wild-type (WT) *Torpedo* AChE (o-o) and the F288L/F290V double mutant (◊-◊). Preincubation with isoOMPA was for 40 minutes are room temperature at the appropriate concentration, and the assay was performed on acetylcholine. Each point represents the average of triplicate assays, and the error bar indicates the extremes for each time point.

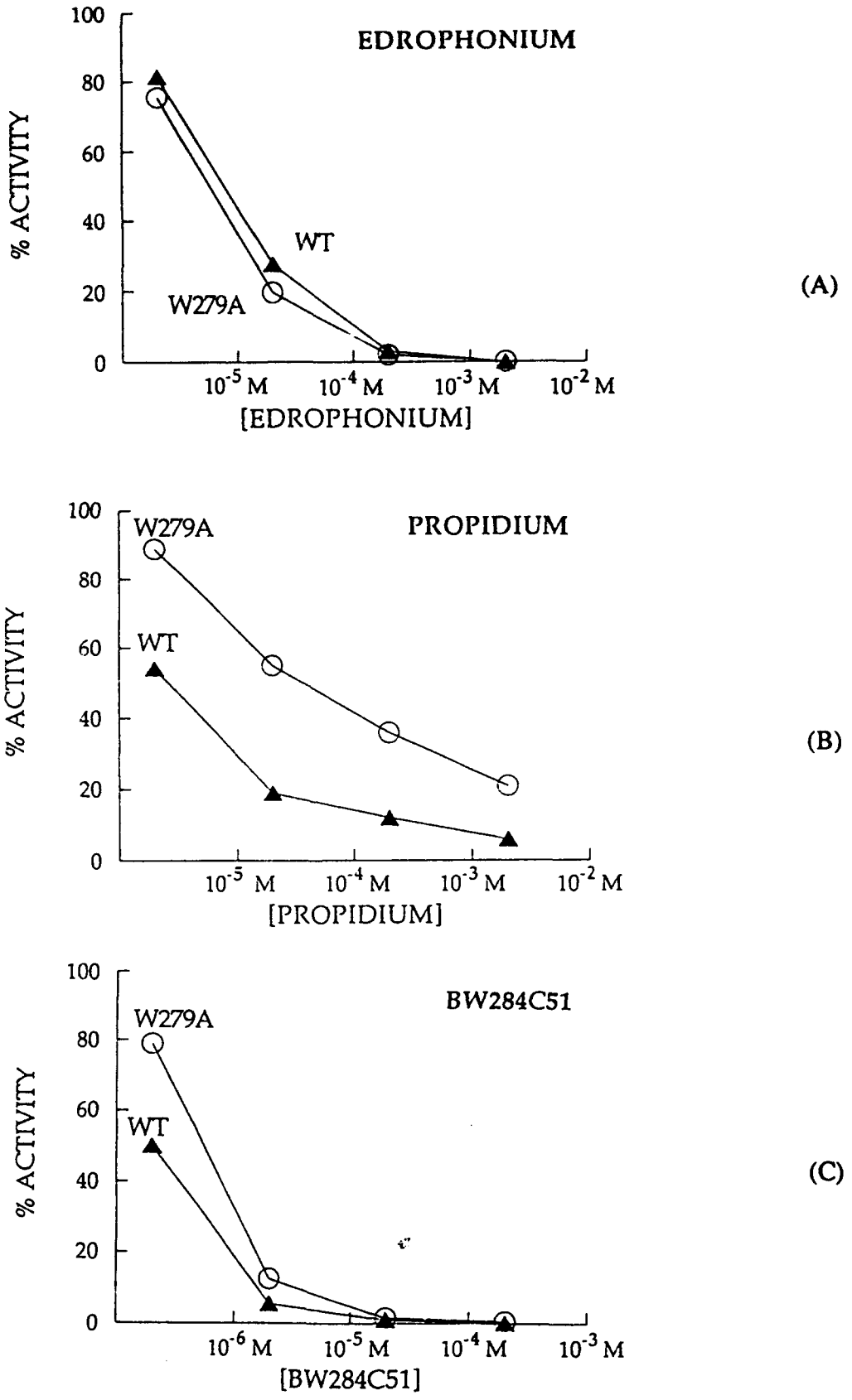

Figure 19. Inhibition of wild-type (WT) *Torpedo* AChE and the W279A mutant by edrophonium (A), propidium (B) and BW284c51 (C).

REFERENCES

1. Neuromuscular Transmission - Enzymatic Destruction of Acetylcholine (1974), Barnard, E. A., in *The Peripheral Nervous System* (J.I. Hubbard, Ed.), pp. 201-224, Plenum, New York.

2. Acetylcholinesterase: Enzyme Structure, Reaction Dynamics, and Virtual Transition States (1987), Quinn, D. M., *Chem. Rev.*, **87**, 955-975.

3. Fractional Diffusion-Limited Component of Reactions Catalyzed by Acetylcholinesterase (1986), Bazelyansky, M., Robey, C. and Kirsch, J. F., *Biochemistry*, **25**, 125-130.

4. Handbuch der Experimentellen Pharmakologie, Vol. 15, Cholinesterase and Anti-cholinesterase Agents (1963), Koelle, G. B., Springer-Verlag, Heidelberg.

5. Anticholinesterase Agents (1990), Taylor, P., in *The Pharmacological Basis of Therapeutics, 5th edition* (A.G. Gilman, A.S. Nies, T.W. Rall and P. Taylor, Ed.), pp. 131-150, MacMillan, New York.

6. Physostigmine, Tacrine and Metrifonate: The Effect of Multiple Doses on Acetylcholine Metabolism in Rat Brain (1989), Hallak, M. and Giacobini, E., *Neuropharmacology*, **28**, 199-206.

7. Acetylcholine Binding by a Synthetic Receptor: Implications for Biological Recognition (1990), Dougherty, D. A. and Stauffer, D. A., *Science*, **250**, 1558-1560.

8. Asymmetric and Globular Forms of Acetylcholinesterase in Mammals and Birds (1979), Bon, S., Vigny, M. and Massoulié, J., *Proc. Natl. Acad. Sci. USA*, **76**, 2546-2550.

9. Chemical and Molecular Basis of Nerve Activity, 2nd edition (1975), Nachmansohn, D. and Neumann, E., Academic Press, New York.

10. Modes of Attachment of Acetylcholinesterase to the Surface Membrane (1987), Silman, I. and Futerman, A. H., *Eur. J. Biochem.*, **170**, 11-22.

11. Ligand Exclusion on Acetylcholinesterase (1990), Berman, H. A. and Leonard, K., *Biochemistry*, **29**, 10640-10649.

12. The Enzymic Hydrolysis and Synthesis of Acetylcholine (1951), Nachmansohn, D. and Wilson, I. B., *Adv. Enzymol.*, **12**, 259-339.

13. Acetylcholinesterase (1971), Froede, H. C. and Wilson, I. B., in *The Enzymes, 3rd edition* (P.D. Boyer, Ed.), pp. 87-114, Academic Press, New York.

14. Acetylcholinesterase (1975), Rosenberry, T. L., *Adv. Enzymol.*, **43**, 103-218.

15. Primary Structure of the Catalytic Subunits from Two Molecular Forms of Acetylcholinesterase (1985), MacPhee-Quigley, K., Taylor, P. and Taylor, S., *J. Biol. Chem.*, **260**, 12185-12189.

16. Acetylcholinesterase VIII. Dissociation Constants of the Active Groups (1950), Wilson, I. B. and Bergmann, F., *J. Biol. Chem.*, **186**, 683-692.

17. Acetylcholinesterase: Studies on Molecular Complementariness (1958), Wilson, I. B. and Quan, C., *Arch. Biochem. Biophys.*, **73**, 131-143.

18. Ligand Binding Properties of Acetylcholinesterase Determined with Fluorescent Probes (1974), Mooser, G. and Sigman, D. S., *Biochemistry*, **13**, 2299-2307.

19. Reactions of 1-Bromo-2-[^{14}C]-pinacolone with Acetylcholinesterase from *Torpedo nobiliana*. Effects of 5-Trimethylammonio-2-pentanone and Diisopropyl Fluorophosphate (1989), Cohen, S. G., Salih, E., Solomon, M., Howard, S., Chishti, S. B. and Cohen, J. B., *Biochim. Biophys. Acta*, **997**, 167-175.

20. Spectral Evidence for the Presence of Tryptophan in the Binding Site of Acetylcholinesterase (1973), Shinitzky, M., Dudai, Y. and Silman, I., *FEBS Lett.*, **30**, 125-128.

21. Inactivation of Electric Eel Acetylcholinesterase by Acylation with N-Hydroxysuccinimide Esters of Amino Acid Derivatives (1978), Blumberg, S. and Silman, I., *Biochemistry*, **17**, 1125-1130.

22. Acetylcholinesterase: Inhibition by Tetranitromethane and Arsenite (1985), Page, J. D. and Wilson, I. B., *J. Biol. Chem.*, **260**, 1475-1478.

23. The Inhibitory Effect of Stilbamidine, Curare and Related Compounds and its Relationship to the Active Groups of Acetylcholine Esterase. Action of Stilbamidine Upon Nerve Impulse Conduction (1950), Bergmann, F., Wilson, I. B. and Nachmansohn, D., *Biochim. Biophys. Acta*, **6**, 217-224.

24. Responses of Acetylcholinesterase from *Torpedo marmorata* to Salts and Curarizing Drugs (1966), Changeux, J. P., *Mol. Pharmacol.*, **2**, 369-392.

25. Interaction of Fluorescence Probes with Acetylcholinesterase. The Site and Specificity of Propidium (1975), Taylor, P. and Lappi, S., *Biochemistry*, **14**, 1989-1997.

26. Role of the Peripheral Anionic Site on Acetylcholinesterase: Inhibition by Substrates and Coumarin Derivatives (1991), Radic, Z., Reiner, E. and Taylor, P., *Mol. Pharmacol.*, **39**, 98-104.

27. Acetylcholinesterase, I. Large-Scale Purification, Homogeneity and Amino Acid Analysis (1967), Leuzinger, W. and Baker, A. L., *Proc. Natl. Acad. Sci. USA*, **57**, 446-451.

28. Acetylcholinesterase: The Structure of Crystals of a Globular Form from the Electric Eel (1975), Chothia, C. and Leuzinger, W., *J. Mol. Biol.*, **97**, 55-60.

29. Crystallization and Preliminary X-Ray Diffraction Analysis of 11 S Acetylcholinesterase (1988), Schrag, J., Schmid, M. F., Morgan, D. G., Phillips, G. N., Jr., Chiu, W. and Tang, L., *J. Biol. Chem.*, **263**, 9795-9800.

30. Comparison of Butyrylcholinesterase and Acetylcholinesterase (1989), Chatonnet, A. and Lockridge, O., *Biochem. J.*, **260**, 625-634.

31. Monographs in Human Genetics, Vol II, Cholinesterase (1986), Whittaker, M., Karger, Basel.

32. Two Selective Inhibitors of Cholinesterase (1953), Austin, L. and Berry, W. K., *Biochem. J.*, **54**, 695-700.

33. Structure and Inhibitors of Cholinesterase (1976), Main, A. R., in *Biology of Cholinergic Function* (A.M. Goldberg and I. Hanin, Ed.), pp. 269-353, Raven Press, New York.

34. Hydrolysis of Suxamethonium by Different Types of Plasma (1969), Hobbiger, F. and Peck, A. W., *Brit. J. Pharmacol.*, **37**, 258-271.

35. Primary Structure of *Torpedo californica* Acetylcholinesterase Deduced from its cDNA Sequence (1986), Schumacher, M., Camp, S., Maulet, Y., Newton, M., MacPhee-Quigley, K., Taylor, S. S., Friedmann, T. and Taylor, P., *Nature*, **319**, 407-409.

36. Profile of the Disulfide Bonds in Acetylcholinesterase (1986), MacPhee-Quigley, K., Vedvick, T. S., Taylor, P. and Taylor, S. S., *J. Biol. Chem.*, **261**, 13565-13570.

37. A Hydrophobic Dimer of Acetylcholinesterase from *Torpedo californica* is Solubilized by Phosphatidylinositol-specific Phospholipase C (1983), Futerman, A. H., Low, M. G. and Silman, I., *Neurosci. Lett.*, **40**, 85-89.

38. Purification and Crystallization of a Dimeric Form of Acetylcholinesterase from *Torpedo californica* Subsequent to Solubilization with Phosphatidylinositol-specific Phospholipase C (1988), Sussman, J. L., Harel, M., Frolow, F., Varon, L., Toker, L., Futerman, A. H. and Silman, I., *J. Mol. Biol.*, **203**, 821-823.

39. The Growth and Preliminary Investigation of Protein and Nucleic Acid Crystals for X-ray Diffraction Analysis (1976), McPherson, A., *Methods Biochem. Analysis*, **23**, 249-345.

40. Atomic Structure of Acetylcholinesterase from *Torpedo californica*: A Prototypic Acetylcholine-Binding Protein (1991), Sussman, J. L., Harel, M., Frolow, F., Oefner, C., Goldman, A., Toker, L. and Silman, I., *Science*, **253**, 872-879.

41. Resolution of Phase Ambiguity in Macromolecular Crystallography (1985), Wang, B. C., in *Diffraction Methods for Biological Macromolecules* (H.W. Wyckoff, C.H.W. Hirs and S.N. Timasheff, Ed.), pp. 90-112, Academic Press, New York.

42. Divergence in Primary Structure between the Molecular Forms of Acetylcholinesterase (1988), Gibney, G., MacPhee-Quigley, K., Thompson, B., Vedvick, T., Low, M. G., Taylor, S. S. and Taylor, P., *J. Biol. Chem.*, **263**, 1140-1145.

43. The Protein Data Bank: a Computer-based Archival File for Macromolecular Structures (1977), Bernstein, F. C., Koetzel, T. F., Williams, G. J. B., Meyer, E. F., Jr., Brice, M. D., Rodgers, J. R., Kennard, O., Schimanouchi, T. and Tasunmi, M., *J. Mol. Biol.*, **112**, 535-542.

44. A Graphics Model Building and Refinement System for Macromolecules (1978), Jones, T. A., *J. Appl. Cryst.*, **11**, 268-272.

45. New Generation Graphics System for Molecular Modeling (1984), Pflugrath, J. W., Saper, M. A. and Quiocho, F. A., in *Methods and Applications in Crystallographic Computing* (S.R. Hall and T. Ashida, Ed.), pp. 404-407, Clarendon Press, Oxford.

46. Using Known Substructures in Protein Model Building and Crystallography (1986), Jones, T. A. and Thirup, S., *EMBO J.*, **5**, 819-822.

47. *Torpedo* Acetylcholinesterase is Inactivated by Thiol agents (1990), Steinberg, N., Roth, E. and Silman, I., *Biochem. Internat.*, **21**, 1043-1050.

48. Solution of a Protein Crystal Structure with a Model Obtained from NMR Interproton Distance Restraints (1987), Brünger, A. T., Campbell, R. L., Clore, G. M., Gronenborn, A. M., Karplus, M., Petsko, G. A. and Teeter, M. M., *Science*, **235**, 1049-1053.

49. Stereochemically Restrained Crystallographic Least-Squares Refinement of Macromolecule Structures (1981), Hendrickson, W. A. and Konnert, J. H., in *Biomolecular Structure, Function, Conformation and Evolution* (R. Srinivasan, E. Subramanian and N. Yathindra, Ed.), pp. 43-57, Pergamon Press, Oxford.

50. Incorporation of Fast Fourier Transforms to Speed Restrained Least-squares Refinement of Protein Structures (1987), Finzel, B. C., *J. Appl. Cryst.*, **20**, 53-55.

51. Addition of Symmetry-Related Contact Restraints to PROTIN and PROLSQ (1987), Sheriff, S., *J. Appl. Cryst.*, **20**, 55-57.

52. Structural Patterns in Globular Proteins (1976), Levitt, M. and Chothia, C., *Nature*, **261**, 552-558.

53. Describing Patterns of Protein Tertiary Structure (1985), Richardson, J. S., in *Diffraction Methods for Biological Macromolecules* (H.W. Wyckoff, C.H.W. Hirs and S.N. Timasheff, Ed.), pp. 341-358, Academic Press, New York.

54. Circular Dichroism Studies of Acetylcholinesterase Conformation. Comparison of the 11 S and 5.6 S Species and the Differences Induced by Inhibitory Ligands (1985), Manavalan, P., Taylor, P. and Johnson Jr., W. C., *Biochim. Biophys. Acta*, **829**, 365-370.

55. Structural and Immunochemical Properties of Fetal Bovine Serum Acetylcholinesterase (1989), Doctor, B. P., Smyth, K. K., Gentry, M. K., Ashani, Y., Christner, C. E., De La Hoz, D. M., Ogert, R. A. and Smith, S. W., in *Computer-Assisted Modeling of Receptor-Ligand Interactions. Theoretical Aspects and Applications to Drug Design* (R. Rein and A. Golombek, Ed.), pp. 305-316, A.R. Liss, New York.

56. Alignment of Amino Acid Sequences of Acetylcholinesterases and Butyrylcholinesterases (1991), Gentry, M. K. and Doctor, B. P., in *Cholinesterases: Structure, Function, Mechanism, Genetics and Cell Biology* (J. Massoulié, F. Bacou, E. Barnard, A. Chatonnet, B.P. Doctor and D.M. Quinn, Ed.), pp. 394-398, American Chemical Society, Washington, DC.

57. Mutagenesis of Essential Functional Residues in Acetylcholinesterase (1990), Gibney, G., Camp, S., Dionne, M., MacPhee-Quigley, K. and Taylor, P., *Proc. Natl. Acad. Sci. USA*, **87**, 7546-7550.

58. Crystallographic and NMR Studies of the Serine Proteases (1982), Steitz, T. A. and Shulman, R. G., *Ann. Rev. Biophys. Bioeng.*, **11**, 419-444.

59. Ser-His-Glu Triad Forms the Catalytic Site of the Lipase from *Geotrichum candidum* (1991), Schrag, J. D., Li, Y., Wu, S. and Cygler, M., *Nature*, **351**, 761-764.

60. The Anatomy and Taxonomy of Protein Structure (1981), Richardson, J. S., *Adv. Protein Chem.*, **34**, 167-339.

61. Single Gene Encodes Glycophospholipid-Anchored and Asymmetric Acetylcholinesterase Forms: Alternative Coding Exons Contain Inverted Repeat Sequences (1990), Maulet, Y., Camp, S., Gibney, G., Rachinsky, T. L., Ekström, T. J. and Taylor, P., *Neuron*, **4**, 289-301.

62. Specific Photoaffinity Labeling Induced by Energy Transfer: Application to Irreversible Inhibition of Acetylcholinesterase (1980), Goeldner, M. P. and Hirth, C. G., *Proc. Natl. Acad. Sci. USA*, **77**, 6439-6442.

63. Anionic Subsites of the Acetylcholinesterase from *Torpedo californica*: Affinity Labelling with the Cationic Reagent *N,N*-Dimethyl-2-phenyl-aziridinium (1990), Weise, C., Kreienkamp, H.-J., Raba, R., Pedak, A., Aaviksaar, A. and Hucho, F., *EMBO J.*, **9**, 3885-3888.

64. Sequence Determination of a Peptide Fragment from Electric eel Acetylcholinesterase, Involved in the Binding of Quaternary Ammonium (1986), Kieffer, B., Goeldner, M., Hirth, C., Aebersold, R. and Chang, J. Y., *FEBS Lett.*, **202**, 91-96.

65. Structural Analysis of Acetylcholinesterase Ammonium Binding Sites (1992), Schalk, I., Ehret-Sabatier, L., Bouet, F., Goeldner, M. and Hirth, C., in *Multidisciplinary Approaches to Cholinesterase Functions* (A. Shafferman and B. Velan, Ed.), pp. 117-120, Plenum Press, New York.

66. Chemical Modification of Electric Eel Acetylcholinesterase by Tetranitromethane (1974), Fuchs, S., Gurari, D. and Silman, I., *Arch. Biochem. Biophys.*, **165**, 90-97.

67. Conformations of Acetylcholine (1968), Chothia, C. and Pauling, P., *Nature*, **219**, 1156-1157.

68. Modification of the Esteratic Activity of Acetylcholinesterase by Alkylation with 1,1-Dimethyl-2-phenylaziridinium Ion (1966), Purdie, J. E. and McIvor, R. A., *Biochim. Biophys. Acta*, **128**, 590-593.

69. On the Irreversible Binding of p-(Trimethylammonium), Benzenediazonium Fluoroborate (TDF) to Acetylcholinesterase from Electrogenic Tissue (1969), Meunier, J.-C. and Changeux, J.-P., *FEBS Lett.*, **2**, 224-226.

70. Hydrophobic Areas on the Active Surface of Cholinesterases (1970), Kabachnik, M. I., Brestkin, A. P., Godovikov, N. N., Michelson, M. J., Rozengart, E. V. and Rozengart, V. I., *Pharmacol. Rev.*, **22**, 355-388.

71. A Hydrophobic Binding Site in Acetylcholinesterase (1975), Steinberg, G. M., Mednick, M. L., Maddox, J., Rice, R. and Cramer, J., *J. Med. Chem.*, **18**, 1056-1061.

72. Chiral Reactions of Acetylcholinesterase Probed with Enantiomeric Methylphosphonothioates (1989), Berman, H. A. and Leonard, K., *J. Biol. Chem.*, **264**, 3942-3950.

73. Chiral Nature of Covalent Methylphosphonyl Conjugates of Acetylcholinesterase (1989), Berman, H. A. and Decker, M. M., *J. Biol. Chem.*, **264**, 3951-3956.

74. Characterization of Peripheral Anionic Site Peptides of AChE by Photoaffinity Labeling with Monoazidopropidium (MAP) (1991), Amitai, G. and Taylor, P., in *Cholinesterases: Structure, Function, Mechanism, Genetics and Cell Biology* (J. Massoulié, F. Bacou, E. Barnard, A. Chatonnet, B.P. Doctor and D.M. Quinn, Ed.), pp. 285, American Chemical Society, Washington, DC.

75. Effective Charge on Acetylcholinesterase Active Sites Determined from the Ionic Strength Dependence of Association Rate Constants with Cationic Ligands (1980), Nolte, H.-J., Rosenberry, T. L. and Neumann, E., *Biochemistry*, **19**, 3705-3711.

76. Structure and Mechanism of Copper, Zinc Superoxide Dismutase (1983), Tainer, J. A., Getzoff, E. D., Richardson, J. S. and Richardson, D. C., *Nature*, **306**, 284-287.

77. Electrostatic Recognition between Superoxide and Copper, Zinc Superoxide Dismutase (1983), Getzoff, E. D., Tainer, J. A., Weiner, P. K., Kollman, P. A., Richardson, J. S. and Richardson, D. C., *Nature*, **306**, 287-290.

78. Structural Basis of Antibody Function (1983), Davies, D. R. and Metzger, H., *Ann. Rev. Immunol.*, **1**, 87-117.

79. Amino Acids of the *Torpedo marmorata* Acetylcholine Receptor α Subunit Labeled by a Photoaffinity Ligand for the Acetylcholine Binding Site (1988), Dennis, M., Giraudat, J., Kotzyba-Hibert, F., Goeldner, M., Hirth, C., Chang, J.-Y., Lazure, C., Chrétien, M. and Changeux, J.-P., *Biochemistry*, **27**, 2346-2357.

80. Identification of a Novel Amino Acid α–Tyrosine 93 within the Cholinergic Ligands-binding Sites of the Acetylcholine Receptor by Photoaffinity Labeling (1990), Galzi, J.-L., Revah, F., Black, D., Goeldner, M., Hirth, C. and Changeux, J.-P., *J. Biol. Chem.*, **265**, 10430-10437.

81. Diffusion Control in Biochemical Reactions (1974), Eigen, M., in *Quantum Statistical Mechanics in the Natural Sciences* (S.L. Mintz and S.M. Widmayer, Ed.), pp. 37-61, Plenum, New York.

82. Interaction of Ligands with Acetylcholinesterase. Use of Temperature-jump Relaxation Kinetics in the Binding of Specific Fluorescent Ligands (1977), Rosenberry, T. L. and Neumann, E., *Biochemistry*, **16**, 3870-3877.

83. Three Dimensional Structure of Acetylcholinesterase (1992), Sussman, J. L., Harel, M. and Silman, I., in *Multidisciplinary Approaches to Cholinesterase Functions* (A. Shafferman and B. Velan, Ed.), pp. 95-107, Plenum Press, New York.

84. Aromatic-Aromatic Interaction: A Mechanism of Protein Structure Stabilization (1985), Burley, S. K. and Petsko, G. A., *Science*, **229**, 23-28.

85. Stereochemistry of Charged Nitrogen-aromatic Interactions and its Involvement in Ligand-receptor Binding (1993), Verdonk, M. L., Boks, G. J., Kooijman, H., Kanters, J. A. and Kroon, J., *Journal of Computer-Aided Molecular Design*, **7** (in press).

86. Inhibition of Cholinesterases by Tetrahydroaminoacridine (1961), Heilbronn, E., *Acta Chem. Scand.*, **15**, 1386-1390.

87. Status of THA as Therapy for Alzheimer's Disease (1991), Gauthier, S. and Gauthier, L., in *Cholinergic Basis of Alzheimer Therapy* (R. Becker and E. Giacobini, Ed.), pp. 224-230, Birkhauser, Berlin.

88. Preparation and Stereochemistry of Some Substituted 4-Thianones and 4-Thianols (1979), Ramalingam, K., Berlin, K. D., Loghry, R. A., van der Helm, D. and Satyamurthy, N., *Journal of Organic Chemistry*, **44**, 477-486.

89. Cholinesterase-like Domains in Enzymes and Structural Proteins: Functional and Evolutionary Relationships and Identification of a Catalytically Essential Aspartic Acid (1991), Krejci, E., Duval, N., Chatonnet, A., Vincens, P. and Massoulié, J., *Proc. Natl. Acad. Sci. USA*, **88**, 6647-6651.

90. Location of Disulfide Bonds Within the Sequence of Human Serum Cholinesterase (1987), Lockridge, O., Adkins, S. and La Du, B. N., *J. Biol. Chem.*, **262**, 12945-12952.

91. Tertiary Templates for Proteins - Use of Packing Criteria in the Enumeration of Allowed Sequences for Different Structural Classes (1987), Ponder, J. W. and Richards, F. M., *J. Mol. Biol.*, **193**, 775-791.

92. Conversion of Acetylcholinesterase to Butyrylcholinesterase: Modeling and Mutagenesis (1992), Harel, M., Sussman, J. L., Krejci, E., Bon, S., Chanal, P., Massoulié, J. and Silman, I., *Proc. Natl. Acad. Sci. USA*, **89**, 10827-10831.

93. Structural Studies on Acetylcholinesterase from *Torpedo californica* (1991), Sussman, J. L., Harel, M., Frolow, F., Oefner, C., Toker, L. and Silman, I., in *Cholinesterases: Structure, Function, Mechanism, Genetics and Cell Biology* (J. Massoulié, F. Bacou, E. Barnard, A. Chatonnet, B.P. Doctor and D.M. Quinn, Ed.), pp. 7-11, American Chemical Society, Washington, DC.

94. The α/β Hydrolase Fold (1992), Ollis, D. L., Cheah, E., Cygler, M., Dijkstra, B., Frolow, F., Franken, S. M., Harel, M., Remington, S. J., Silman, I., Schrag, J., Sussman, J. L., Verschueren, K. H. G. and Goldman, A., *Protein Eng.*, **5**, 197-211.

95. On the Specificity of Antibody/Antigen Interactions: Phosphocholine Bindng to McPC603 and the Correlation of Three-Dimensional Structure and Sequence Data (1985), Padlan, E. A., Cohen, G. H. and Davies, D. R., *Ann. Inst. Pasteur/Immunol.*, **136C**, 271-276.

96. Structure of the Agonist-binding Site of the Nicotinic Acetylcholine Receptor. [^{3}H]-Acetylcholine Mustard Identifies Residues in the Cation-Binding Subsite (1991), Cohen, J., Sharp, S. D. and Liu, W. S., *J. Biol. Chem.*, **266**, 23354-23364.

97. Allosteric Transitions of the Acetylcholine Receptor Probed at the Amino Acid Level with a Photolabile Cholinergic Ligand (1991), Galzi, J.-C., Revah, F., Bouet, F., Ménez, A., Goeldner, M., Hirth, C. and Changeux, J.-P., *Proc. Natl. Acad. Sci. USA*, **88**, 5051-5055.

98. Acetylcholinesterase: Structure and Use as a Model for Specific Cation-protein Interactions (1992), Sussman, J. L. and Silman, I., *Curr. Opin. Struct. Biol.*, **2**, 721-729.

99. The Use of an Imaging Proportional Counter in Macromolecular Crystallography (1987), Howard, A. J., Gilliland, G. L., Finzel, B. C., Poulos, T. L., Ohlendorf, D. H. and Salemme, F. R., *J. Appl. Cryst.*, **20**, 383-387.

100. Evaluation of Single-Crystal X-ray Diffraction Data from a Position-Sensitive Detector (1988), Kabsch, W., *J. Appl. Cryst.*, **21**, 916-924.

101. A Least-Squares Refinement Method for Isomorphous Replacement (1968), Dickerson, R. E., Weinzierl, J. E. and Palmer, R. A., *Acta Cryst.*, **B24**, 997-1001.

102. *RIBBON*: a Stereo Cartoon Drawing Program for Proteins (1988), Priestle, J. P., *J. Appl. Cryst.*, **21**, 572-576.

103. γ–Chymotrypsin is a Complex of α–Chymotrypsin with its Own Autolysis Products (1991), Harel, M., Su, C. T., Frolow, F., Silman, I. and Sussman, J. L., *Biochemistry*, **30**, 5217-5225.

VIII) LIST OF PUBLICATIONS RESULTING FROM THIS CONTRACT

Published Papers

1. J.L. Sussman, M. Harel, F. Frolow & I. Silman (1989). "X-ray crystallographic studies of acetylcholinesterase." *Proc. 1989 U.S. Army Medical Defense Bioscience Review*, Columbia, MD, 309-316.

2. N. Steinberg, E. Roth & I. Silman (1990). "*Torpedo* acetylcholinesterase is Inactivated by Thiol Agents." *Biochem. Internat.* **21**, 1043-1050.

3. J.L. Sussman, M. Harel, F. Frolow, C. Oefner, L. Toker & I. Silman (1991). "Structural Studies on Acetylcholinesterase from *Torpedo californica*." In *Cholinesterases: Structure, Function, Mechanism, Genetics, and Cell Biology* (J. Massoulié, F. Bacou, E. Barnard, A. Chatonnet, B.P. Doctor & D.M. Quinn, eds.), 7-11.

4. J.L. Sussman (1991). "Introduction to Macromolecular Refinement." In *Crystallographic Computing*, **5**, (D. Moras, A.D. Podjarny & J.C. Thierry, eds), Oxford Univ. Press, New York, 382-391.

5. M. Harel, C.-T. Su, F. Frolow, I. Silman & J.L. Sussman (1991). "γ-Chymotrypsin is a Complex of α-Chymotrypsin With its Own Autolysis Products." *Biochemistry* **30**, 5217-5225.

6. J.L. Sussman, M. Harel, F. Frolow, C. Oefner, A. Goldman, L. Toker & I. Silman (1991). "Atomic Structure of Acetylcholinesterase from *Torpedo californica*: A Prototypic Acetylcholine-Binding Protein." *Science* **253**, 872-879.

7. M. Harel, C.-T. Su, F. Frolow, Y. Ashani, I. Silman & J.L. Sussman (1991). "The Refined Crystal Structures of 'Aged' and 'Non-Aged' Organophosphoryl Conjugates of γ-Chymotrypsin." *J. Mol. Biol.* **221**, 909-918.

8. J.L. Sussman, M. Harel, F. Frolow, A. Goldman, C. Oefner, L. Toker & I. Silman (1991). "3-D Structure of Acetylcholinesterase from *Torpedo californica*." *Proc. 1991 U.S. Army Medical Defense Bioscience Review*, Aberdeen Proving Ground, MD, 441-448.

9. D.L. Ollis, E. Cheah, M. Cygler, B. Dykstra, F. Frolow, S.M. Fraken, M. Harel, S.J. Remington, I. Silman, J. Schrag, J.L. Sussman, K.H.G. Verschueren & A. Goldman (1992). "The α/β Hydrolase Fold." *Protein Engineering* **5**, 197-211.

10. A. N. Pryor, T. Selwood, L.-S. Leu, M. A. Andracki, B. H. Lee, M. Rao, T. Rosenberry, B. P. Doctor, I. Silman & D. M. Quinn (1992). "Simple General Acid, Base Catalysis of Physiological Acetylcholinesterase Reactions." *J. Am.. Chem.. Soc.* **114**, 3897-3900.

11. A. Shafferman, C. Kronman, Y. Flashner, M. Leitner, H. Grosfeld, A. Ordentlich, Y. Gozes, S. Cohen, N. Ariel, D. Barak, M. Harel, I. Silman, J. L. Sussman & B. Velan (1992). "Mutagenesis of Human Acetylcholinesterase. Identification of Residues Involved in Catalytic Activity and in Polypeptide Folding." *J. Biol. Chem.* **267**, 17640-17648.

12. N. Duval, S. Bon, I. Silman, J.L. Sussman & J. Massoulié (1992). "Site-directed Mutagenesis of Active-site-related Residues in *Torpedo* Acetylcholinesterase. Presence of a Glutamic Acid in the Catalytic Triad." *FEBS Letts.* **309**, 421-423.

13. J.L. Sussman, M. Harel & I. Silman (1992). "3-D Structure of Acetylcholinesterase and Complexes of it with Anticholinesterase Agents." In *Membrane Proteins: Structures, Interactions and Models - The Jerusalem Symposia on Quantum Chem. and Biochem.*, Vol. 25 (A. Pullman, J. Jortner & B. Pullman, eds.), Kluwer Academic Publishers, Dordrect, Holland, 161-175.

14. I. Silman, M. Harel, E. Krejci, S. Bon, P. Chanal, J.L. Sussman, & J. Massoulié (1992). "Modelling and Mutagenesis of Butyrylcholinesterase Based on the X-ray Structure of Acetylcholinesterase." In *Membrane Proteins: Structures, Interactions and Models - The Jerusalem Symposia on Quantum Chem. and Biochem.*, Vol. 25 (A. Pullman, J. Jortner & B. Pullman, eds.), Kluwer Academic Publishers, Dordrect, Holland, 177-184.

15. J.L. Sussman, M. Harel & I. Silman (1992). "Three-Dimensional Structure of Acetylcholinesterase." In *Multidisciplinary Approaches to Cholinesterase Functions* (A. Shafferman & B. Velan, eds.), 95-107.

16. M. Cygler, J.D. Schrag, J.L. Sussman, M. Harel, I. Silman, M.K. Gentry & B.P. Doctor (1992). "Sequence Alignment of Esterases and Lipases Based on 3-D Structure of Two

Members of this Family." In *Multidisciplinary Approaches to Cholinesterase Functions* (A. Shafferman & B. Velan, eds.), 109-116.

17. D. M. Quinn, T. Selwood, A. N. Pryor, B. H. Lee, L.-S. Leu, S. A. Acheson, I. Silman, B.P. Doctor & T. L. Rosenberry (1992). "Cryptic Catalysis and Cholinesterase Function." In *Multidisciplinary Approaches to Cholinesterase Functions* (A. Shafferman & B. Velan, eds.), 141-148.

18. I. Silman, E. Krejci, N. Duval, S. Bon, P. Chanal, M. Harel, J.L. Sussman & J. Massoulié (1992). "Site-Directed Mutagenesis of Functional Residues in *Torpedo* Acetylcholinesterase." In *Multidisciplinary Approaches to Cholinesterase Functions* (A. Shafferman & B. Velan, eds.), 177-183.

19. M. Harel, I. Silman & J.L. Sussman (1992). "A Model of Butyrylcholinesterase Based on the X-ray Structure of Acetylcholinesterase Indicates Differences in Specificity." In *Multidisciplinary Approaches to Cholinesterase Functions* (A. Shafferman & B. Velan, eds.), 189-194.

20. J. Massoulié, J.L. Sussman, B.P. Doctor, H. Soreq, B. Velan, M. Cygler, R. Rotundo, A. Shafferman, I. Silman, & P. Taylor (1992). "Recommendations for Nomenclature in Cholinesterases." In *Multidisciplinary Approaches to Cholinesterase Functions* (A. Shafferman & B. Velan, eds.), 285-288.

21. J.L. Sussman & I. Silman (1992). "Acetylcholinesterase: Three-Dimensional Structure and Use as a Model for Studying Specific Cation-Protein Interactions." *Current Opinion in Structural Biol.* **2**, 721-729.

22. M. Harel, J.L. Sussman, E. Krejci, S. Bon, P. Chanal, J. Massoulié & I. Silman (1992). "Conversion of Acetylcholinesterase to Butyrylcholinesterase: Modeling and Mutagenesis." *Proc. Natl. Acad. Sci. USA* **89**, 10827-10831.

23. R.C. Tan, T.N. Truong, J. A. McCammon & J.L. Sussman (1993). "Acetylcholinesterase: Electrostatic Steering Increases the Rate of Ligand Binding." *Biochemistry* **32**, 401-403.

24. J.L. Sussman, M. Harel & I. Silman (1993). "Three-dimensional Structure of Acetylcholinesterase and of its Complexes with Anti-cholinesterase Drugs." Proceedings

2nd Internat. Meeting on Esterases Hydrolyzing Organophosphorus Compounds, Salsomaggiore, 1992, *Chemico-Biological Interactionss*, in press.

25. J. Massoulié, J.L. Sussman, S. Bon & I. Silman (1993). "Structure and Functions of Acetylcholinesterase and Butyrylcholinesterase." Symposium on Cholinergic Neurotransmission: Function and Dysfunction, Montreal, 1992, *Progress. Neurobiol.*, in press.

26. M. Cygler, J.D. Schrag, J.L. Sussman, M. Harel, I. Silman, M.K. Gentry & B.P. Doctor (1993). "Relationship Between Sequence Conservation and Three-dimensional Structure in a Large Family of Esterases, Lipases, and Related Proteins." *Protein Sci* **2**, 366-382.

27. D.R. Ripoll, C.H. Faerman, P. Axelsen, I. Silman & J.L. Sussman (1993). "An Electrostatic Mechanism of Substrate Attraction in Acetylcholinesterase." *Proc. Natl. Acad. Sci. USA* **90** (in press).

28. M. Harel, K. Schalk, L. Ehret-Sabatier, F. Bouet, M. Goeldner, C. Hirth, P. Axelsen, I. Silman & J.L. Sussman (1993). "Quaternary Ligand Binding to Aromatic Residues in the Active-site Gorge of Acetylcholinesterase." *Proc. Natl. Acad. Sci. USA* **90** (in press).

29. J. Eichler, A. Anselmet, J. L. Sussman, J. Massoulié & I. Silman (1993). "Differential Effects of 'Peripheral' site Ligands on *Torpedo* and Chicken Acetylcholinesterase." *Mol. Pharmacol.* (submitted).

Contributions to the Brookhaven Protein Data Bank

1. M. Harel, I. Silman & J.L. Sussman (1991). Refined γ-Chymotrypsin Structure at 1.9 Å resolution (Accession No. 8GCH).

2. J.L. Sussman, M. Harel Silman (1993). *Torpedo californica* Acetylcholinesterase at 2.8 Å resolution (Accession No. 1ACE).

3. M. Harel, I. Silman & J.L. Sussman (1993). Organophosphoryl complexes of γ-Chymtrypsin at 1.9 Å Resolution (in preparation).

IX) List of Personnel

Prof. Israel Silman (Ph.D.)

Prof. Joel L. Sussman (Ph.D.)

Dr. Michal Harel (Ph.D.)

Dr. Ulrike Wagner (Ph.D.)

Dr. Nitza Steinberg (Ph.D.)

Dr. Felix Frolow (Ph.D.)

Dr. Oded Livnah (Ph.D.)

Lilly Toker (M.Sc.)

Alexander Faibusovich (M.Sc.)

Richard Cormack (M.Sc.)

Yaacov Halfon (B.Sc.)

Jerry Eichler (M.Sc.)

Miriam Laschever (B.Sc.)

Mira Ben-Ami (B.Sc.)